ENOS

Enabling Onshore CO_2 Storage

A CO_2GeoNet Initiative

ENOS D2.3 | v2.1

High resolution Dynamic modelling of heterogeneous Reservoirs

Date	10.10.2019
Author(s)	Muhammad Adeel Nasser Sohal, Sean Rigby, University of Nottingham, UK

Number of pages	39
Number of appendices	0
Customer	EC
Project name	ENOS
Project number	GA No 653718

This project has received funding from the European Union's Horizon 2020 research and innovation programme under grant agreement No 653718.

Table des matières

1 Executive Summary

The deliverable from this work has been the effect of geological heterogeneities, and fault transmissibilities, on storage and potential redirection of the CO_2 plume during a long term CO_2 injection process. The Hontomín geological model was used to provide the deliverable D2.3 for task 2.1.1. Modelling work was carried out on the original model with 100 × 100 m dimensions in the X and Y directions to assess the impact of geological heterogeneities (e.g. permeability anisotropy, porosity, fault transmissibilities etc.). The Hontomín simulation model was validated with water alternating gas injection data from 2017, prior to the predictive simulations. A near wellbore refined model was used for the simulation sensitivity study. Bugs in the Intersect software, related to use of two-phase (gas-water) relative permeability, limited its use in this work package and delayed the validation process, as described in detail in the report. As a consequence, only tens of different realisations were possible, instead of the intended hundreds. A sensitivity study was performed using the Eclipse compositional reservoir simulation program. The findings from the simulation study improved the understanding of the impact of geological heterogeneities and fault transmissibilities on the movement of the CO_2 plume during long term injection campaigns. Predictive simulations were run for 30 to 200 years hence, replicating the historical injection schemes. Simulation sensitivity studies indicated that, by changing the reservoir matrix and fracture directional permeabilities, the direction of the CO_2 plume movement was impacted, as well as the reservoir pressure. The reservoir storage capacity was significantly sensitive to the matrix porosity and permeability heterogeneity. A sensitivity study, to assess the impact of permeability heterogeneity on reservoir storage capacity and CO_2 plume migration, was performed in a volume control mode. The volume control mode provides a more dynamic view of the reservoir storage capacity with time variation amongst the heterogeneous models compared to the direct estimation of injected volume in pressure control mode. It was observed that, the reservoir storage capacity and the direction of CO_2 plume migration is different amongst the simulated heterogeneous cases at similar pressure and porosity. In the reservoir simulation study, the flow of fluid through the faults is controlled by the fault transmissibility multiplier. In this study the reservoir pressure and the movement of CO_2 plume seemed insensitive to fault transmissibilities. This means that the gas flow was not affected in both fully transmissive and sealing fault scenarios, and therefore a change in injection pressure was not observed. The possible reason could be the CO_2 plume front was far away from most of the fault boundaries. However, a response was observed in the pressure due to fault F11 and R4+5 transmissibilities when the CO_2 plume reached their vicinity. The impact of other faults on injection and reservoir pressures could not be detected as they are located far away from the plume location even after 200 years of injection. The 100 years of injection resulted in the reservoir pressure increasing from 140 to 152 bars.

It is observed that by decreasing the reservoir matrix permeability close to zero for some layers which is normally observed in geological features like granulation seams, cemented fault zones etc., reservoir storage capacity significantly decreases. In the simulation study of randomly distributed matrix permeability cases, the case base_41 with high permeability distribution among the layers can store 2.9×10^5 tons of CO_2 which is 4.6 times more compared to the case base_31 which stored 4.5×10^4 tons and has low permeability distribution among the layers on reaching a similar reservoir pressure (14800 kPa). The high permeability case would take approximately 27 years additional injection time at the same injection rate to reach the same reservoir pressure.

Similarly, when the fracture permeability was doubled, compared to the base case, in either the X or Y direction, the reservoir storage capacity increased 1.86, and 2.48 times, respectively, compared to the base case. The same trend was observed when matrix permeability in either the X or Y direction was doubled compared to the base case, since then the reservoir storage capacity increased by 44% or 51%, respectively. These calculations are based on reservoir pressure against the injection rate. Therefore, the injection period necessary was larger for good permeability cases compared to poor permeability cases to reach the same reservoir pressure level.

2 Context of the work and limitations

The present work was performed in the frame of the ENOS project, Work Package 2, task 2.1. 1 High resolution dynamic modelling of heterogeneous Reservoirs.

This model will be used to simulate the impact of heterogeneities (at reservoir scale) on the storage of CO_2 and the potential redirection of the injected plume. It will be modelled in a single, unified simulation incorporating dual and single permeability options.

In this study, the Hontomín geological model was initially validated with brine injection and WAG well test data, in order to subsequently investigate the influence of geological heterogeneities on movement of CO_2 plume and reservoir storage capacity in a long-term CO_2 injection plan. In these subsequent investigations the impact of permeability anisotropy, porosity, and fault transmissibilities were observed. Moreover, completely heterogeneous models were developed by using sequential Gaussian simulation method to populate the grid cell with different permeability values. Furthermore, the effect of faults transmissibility on movement of CO_2 plume and on reservoir pressure were investigated during a long-term CO_2 injection process.

The attempts to use commercial Schlumberger software for this work package led to the discovery of a series of bugs in both the Intersect (IX) and Eclipse software packages, as successive solutions were attempted, as will be described below. The static geological model of Hontomín site was supposed to be validated with observed water alternating gas injection data in INTERSECT. However, IX cannot simulate a compositional case with only gas-water relative permeability [(1)] input. Therefore, a water alternating gas (CO_2) process could not be simulated using the CO2STORE keyword, as suggested by Schlumberger. The WAG 2017 data, which was provided along with the static geological model, showed simultaneous injection of water and CO_2 for a short period of time (≈20 min) especially during the fluid exchange interval as shown in Figure 1. The intervals of simultaneous injection of water and CO_2 were reduced to run the simulations in a good time.

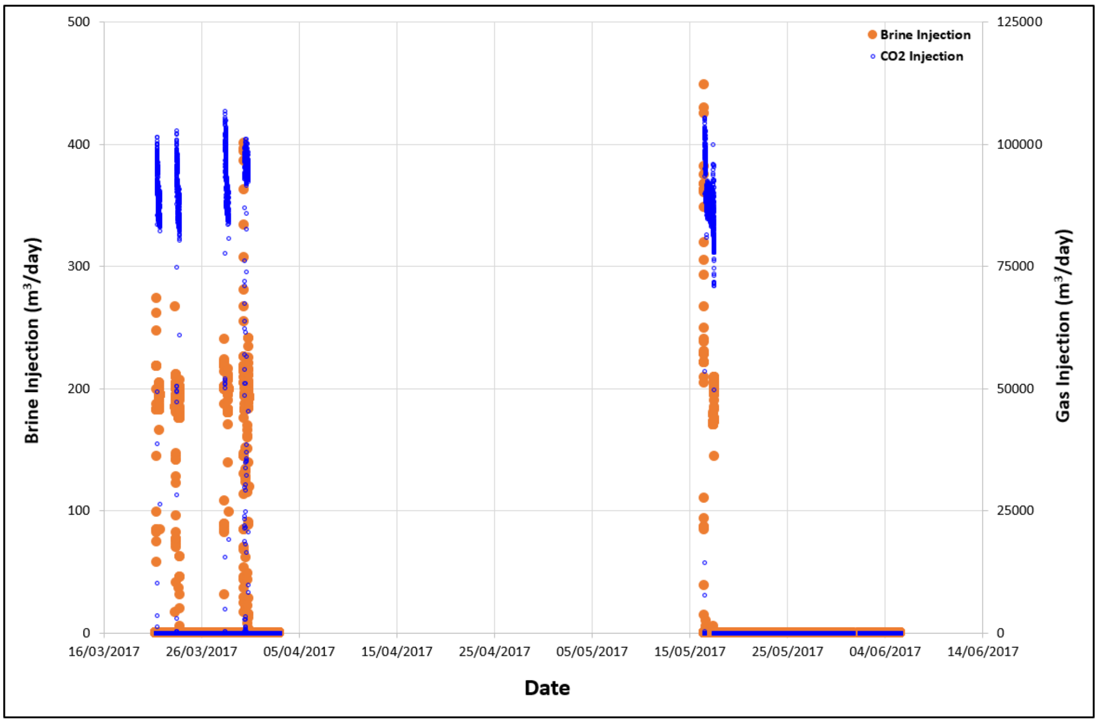

Figure 1. Intervals of simultaneous injection of Brine and CO_2 in WAG observed data, 2017.

The model validation commenced with Eclipse 300 by using the WSF, GSF and CO2STORE keywords family, as suggested by Schlumberger [(2)]. Schlumberger said it is this keyword family which is commonly used to simulate carbon dioxide storage problems within deep saline aquifers. In this keyword family only gas-water relative permeability is used to control the gas and water mobility in reservoir. However, the WCONINJH keyword, which declares the injection wells as a special history matching wells, produced a bug. The brine injection well (HI-W) in the WAG process was injecting water equal to gas injection rate because of a bug associated with the WCONINJH keyword. The bug was referred to Schlumberger and they promised to fix it in the next version of the software. However, they did not provide any time frame for the release of the next version. Subsequently, the WCONINJE keyword was used to model the brine and CO_2 injection rates along with the WSF, GSF and CO2STORE keywords family. However, the model was then insensitive to any change in the (critical) reservoir parameters (e.g., Fracture and matrix permeability, matrix porosity, relative permeability, capillary pressure etc.) during the history matching process. Once more Schlumberger were consulted, and unfortunately were unable to provide an immediate solution for this problem [(3)]. However, after a couple of weeks, Schlumberger determined that the issue was originating by ignoring the ACTNUM keyword for fractures. However, before that response had been provided by Schlumberger, the SWFN, SGFN, SOF3 keyword family had been applied to simulate the WAG injection case since there is an option to add gas-water capillary pressure in this keyword family. The oil relative permeability is an essential input parameter and cannot be ignored in this keyword family. However, as there was, of course, no actual oil phase present in Hontomín case as it is a saline aquifer model; it was attempted to simulate the system with very low oil relative permeability values (10^{-7}). However, Eclipse internally adjusted the relative permeabilities of all the phases by default, as described by Schlumberger [(3)]. Therefore, it was not feasible to simulate the model with this option. In addition to all the various different approaches described above, an alternative approach, which is explained in [(4, 5)], was also pursued. In this method, the compositional simulation case (E300) was simulated using a black oil simulator (E100) by converting the fluid model. The conversion of the compositional fluid model into a black oil case was achieved by using TOUGH2 software, which is a numerical simulation program for non-isothermal flows of multicomponent, multiphase fluids in porous and fractured media. It was developed by the Department of Energy Office of Scientific and Technical Information (OSTI.GOV) of the United States. Once more the proposed approach was discussed with Schlumberger, but they recommended to avoid this method since there is no guarantee that the black oil model will accurately reproduce the compositional behaviour [(6)]. Additionally, this method is not suitable to run the sensitivity studies.

Finally, the SWOF and SGOF keyword family of E300 was recommended by Schlumberger [(7)]. The simulations proceeded well with this keywords family without oil phase in the system. The oil relative permeability was set to zero, which did not affect the CO_2-brine simulation results as illustrated by Schlumberger [(7)]. They explained that the capillary pressure (Pc) for oil-water phases could be added under the SWOF keyword which is internally converted by the program for gas-water phases if there is no oil phase present in the system [(7)]. The gas-oil and water-oil capillary pressures are added through SGOF and SWOF keywords. However, if there is no oil phase in the system then gas-water capillary pressure could be entered under SWOF keyword instead of water-oil and gas-oil capillary pressure is set to zero in SGOF keyword. However, on applying the local grid refinement (LGR) around the injection well, the transmissibility of adjacent global grids became zero in E300, but CO_2 was flowing through the cells. This further problem was passed on to Schlumberger. Schlumberger responded that this problem may be due to yet another BUG, although this is not confirmed yet, and needs further investigation, which is ongoing. However, Schlumberger did suggest the issue was related to a display problem inside the Petrel package, since the transmissibility of the relevant cells was not actually zero as CO_2 was flowing through the cells. This series of issues with the commercial software slowed progress. The final methodology developed was found to work in both E300 and IX. Multi-million cell models were also possible and were attempted.

3 Modelling Approach

In this study, the effect of geological heterogeneities on the flow of a CO_2 plume was investigated during long term storage within the Sopeña Formation, which is a deep saline aquifer. Since the Sopeña Formation is highly fractured it was simulated by using the dual permeability option within E300. The Hontomín geological model has already been thoroughly explained in D1.3. In this study, the homogeneous reservoir model was initially further constrained with the WAG well-test data, and then the resultant model was used for simulations of long-term CO_2 injection to achieve the WP2 objectives. During long term CO_2 injection, the effect of heterogeneities such as vertical to horizontal permeability ratio (kv/kh), fault transmissibilities, and random variation in matrix and fractures permeability in direction and magnitude were explored. The dimensions of the Sopeña formation in the Hontomín geological model are 5.7 km by 5.6 km with a thickness of 120 m. The horizontal matrix permeability (kh) is 0.5 md, the vertical matrix permeability (kv) was set to 0.05 md, and the porosity varies from 3 to 13% in original model. The model was considered initially in static equilibrium, with an initial reservoir pressure of 141 bar at a Subsea True Vertical Depth (SSTVD) of 494 m. The initial water saturation (Sw) was 100% and the salinity of the formation water was 40000 ppm. There was no dissolved gas in the aqueous phase at the beginning of the simulation. The reservoir was modelled with 40 layers, and the thicknesses of layers varied from 1 to 10 m. The Hontomín geological model was uniformly gridded in the three principal directions with 57 cells in X-direction, 56 in y-directions and 658 cells in the Z-direction. The reservoir model details are summarized in Table 1.

Table 1. Details of the validated homogeneous simulation model of Hontomín site.

Parameters	Values	Units
Total Grid Cells	2103528	
Reservoir length	5.7	Km
Reservoir width	5.6	Km
Reservoir thickness	120	m
Dip		
Original matrix horizontal permeability	0.5	mD
Original matrix vertical permeability	0.05	mD
Matrix porosity	3 to 13	%
Fracture permeability in X- direction	240	mD
Fracture permeability in Y- direction	310	mD
Fracture permeability in Z- direction	310	mD
Fracture porosity	0.01	
Net to gross ratio	1	
Sigma	1	
Reservoir depth (SSTVD)	494	m
Reservoir pressure	141	bar
Reservoir temperature	42	oC
Initial water saturation	1	
Residual water saturation	10	%
Water endpoint relperm	1	
Residual gas saturation	0.05	%
Gas end point relperm	0.9	
Pore brine salnity	40000	ppm
Components	H2O, CO2	
Pore brine density	1.002	g/cm^3
Formation volume factor	1.01	Rm^3/Sm^3
Pore brine viscosity	0.66	cP

3.1 Relative Permeability and P_c Data

In the literature, different CO_2–Brine relative permeability curves for carbonate rocks have been proposed, but the following set of drainage relative permeability curves, measured in Wabamun Limestone Formation by Bennion and Bachu [9], was initially used in this simulation study. However, the relative permeabilities for matrix and fractures were further adjusted with the help of Corey's model [10] for gas water system as given in equations (1) and (2).

$$K_{rg} = K_{rg(wir)} \left[\frac{S_g - S_{gr}}{1 - S_{gr} - S_{wir}} \right]^{ng} \qquad (1)$$

$$K_{rw} = K_{rw(gr)} \left[\frac{S_w - S_{wir}}{1 - S_{gr} - S_{wir}} \right]^{nw} \qquad (2)$$

Where S_{wir} is the irreducible water saturation, which was set to 0.1. The residual CO_2 saturation S_{gr} was 0.05, and the water (nw) and CO_2 (ng) Corey's functions were equal to 1 and 2, respectively. In the initial model validation process, the same relative permeability curves were used to model CO_2 displacing water and water displacing CO_2 (i.e., no hysteresis in relative permeability). The final relative permeability curves for matrix and fractures are shown in Figure 2.

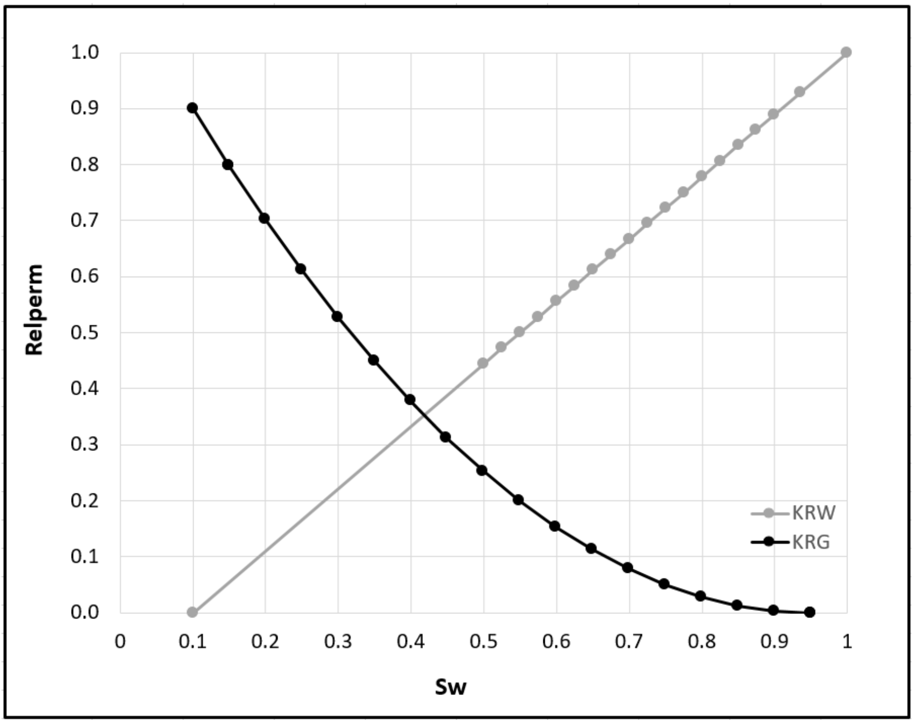

Figure 2. The relative permeability curves for matrix and fractures that used in the history matching process.

In the petrophysical lab report that was provided with the geological model 38% to 78% of the pore throats of Sopeña Formation are in the IUPAC micropore scale (< 2 nm) range.

Therefore, the pore entry pressure (capillary pressure) for the majority of the rock pores is greater than the CO_2 injection pressure. Consequently, CO_2 will not invade a significant part of the reservoir rock during the injection period and principally migrate through the fractures. The capillary pressure used in the simulation study was calculated in Petrel and maximum value was manually adjusted to match with the observed data. Petrel calculates the capillary pressure function using a correlation for mixed-wet reservoir rock from the simple power-law form of Brooks and Corey [(11)] as given in equation (3):

$$p_c = \frac{c_w}{\left(\frac{S_w - S_{wR}}{1 - S_{wR}}\right)^{a_w}} + \frac{c_o}{\left(\frac{S_o - S_{oR}}{1 - S_{oR}}\right)^{a_o}} \qquad (3)$$

Where c_w is the entry pressure for the water phase, c_o is the entry pressure for the gas phase if there is no oil phase, a_w and a_o is pore size distribution for water and oil phases, S_{wR} is the residual water saturation, S_{oR} is the residual oil saturation, and S_w and So are the water and oil saturations respectively. The final capillary pressure curve for the matrix and fractures is depicted in Figure 3. In this case water is the wetting phase and displaced by CO_2 which is a non-wetting phase. Thus, the capillary pressure relationship given in Figure 3 is for primary drainage, meaning that the wetting phase (water) is decreasing from an initial value of 100%. Gas does not penetrate the medium, as shown in Figure 3, until the capillary pressure exceeds the threshold pressure (P_{ct}) limit. This pressure limit is not significantly high for the Sopeña Formation, which is a fractured carbonate reservoir.

It is noted that Schlumberger advised that Eclipse E300 can internally change the P_{cow} into P_{cgw} if there is no oil phase in the system, as explained in previous section. During the history matching process, a better match of the observed data was difficult to achieve without adding a capillary pressure curve.

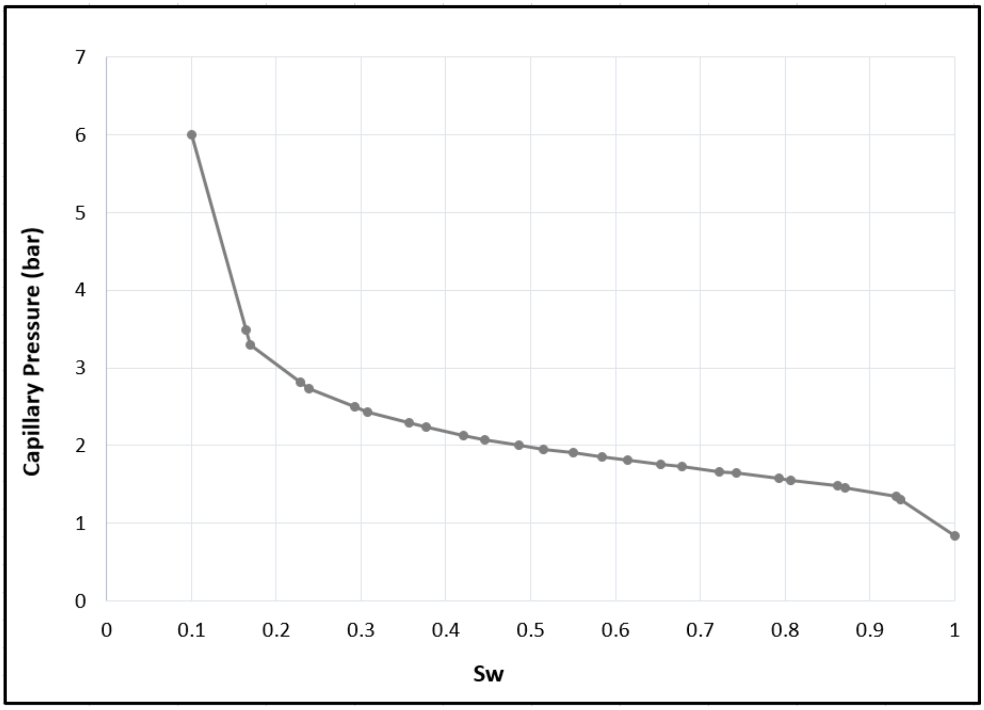

Figure 3. Capillary pressure curve used in the history matching process.

3.2 Constrained Hontomín Simulation Model

The Hontomín model was first constrained with the brine well-test data from 2017, to adjust the reservoir matrix and fracture permeabilities, as described in the WP1 report. In that previous history matching process, the relative permeability and capillary pressure data were not required since only a single phase (brine) was flowing through the rock pores. However, relative permeability and capillary pressure curves were used for the complete history matching process using both the brine and WAG well-test data from 2017. History matching was commenced with the Petrel uncertainty and optimization workflow, but the match was then further improved manually. The match between the simulated and observed bottom-hole pressures could be potentially further improved, but program limitations and bugs delayed the history matching process. The reservoir bottom-hole pressure in the observed data for last WAG slug is inconsistent with prior slugs, since it should increase, as more gas is being injected into the reservoir, instead of decreasing. Consequently, Pressure mismatch in the last WAG slug is greater compared to all the other observed data as can be seen in Figure 4. In this validation process LGR and capillary pressure were added, otherwise it would not have been possible to get a better match.

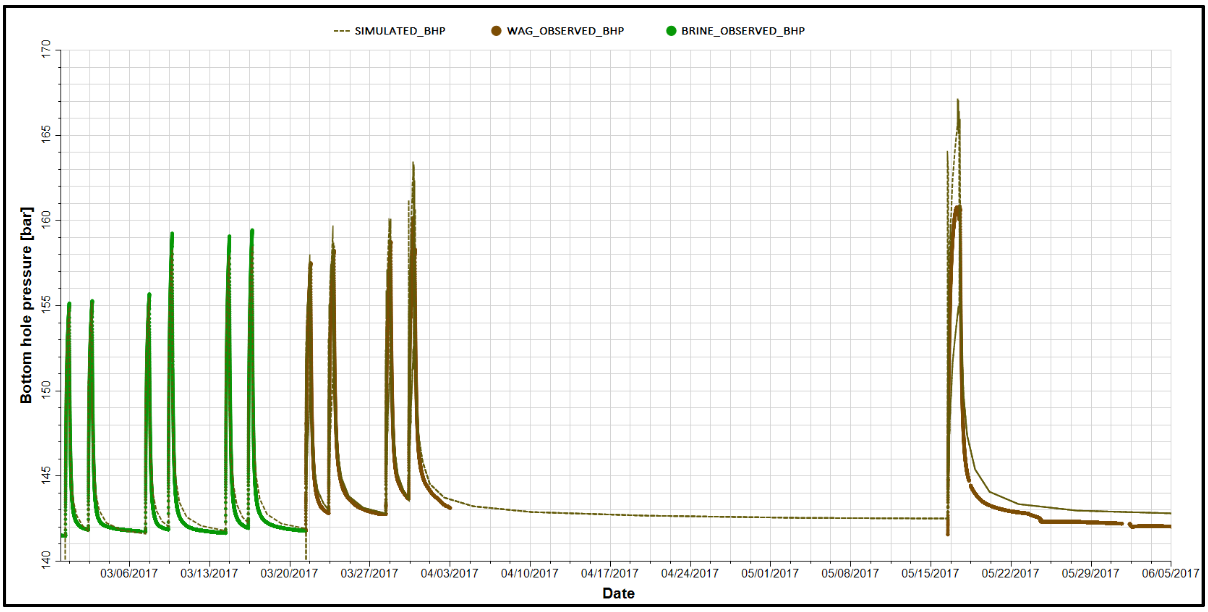

Figure 4. History matched bottom-hole pressure of Hontomín model with brine and WAG observed data for 2017.

4 Simulation Results for Homogeneous Model

In the original Hontomín geological model, the permeability of the limestone and dolomite facies was approximately 0.5 mD and almost constant throughout the Sopeña reservoir. As a result of the well-test history matching process, the matrix permeability was increased up to 2 mD, but it was still constant throughout the described facies. Therefore, all of the forty layers of the Sopeña reservoir were equally likely for CO_2 migration. Fracture permeabilities within the Sopeña reservoir were set to 23 % higher in E-W direction compared to N-S direction. It has been identified, by Le Gallo and de Dios (12) in Tele-viewer log interpretation, that the number of fractures in the E-W (278) direction is greater than the number of fractures in the N-S (48 fractures) direction. Historical data showed that slugs of brine and CO_2 had been injected into the Sopeña Formation and the average injected volume of brine and gas in each slug was approximately 21 and 28333 sm^3 for brine and CO_2 respectively. Cumulative slug injection volumes for one whole year were converted into injection rates per day, which became approximately 6 sm^3/day for brine and 8151 sm^3/day for gas, respectively. During a slug injection process, a large volume of gas is injected over a small period of time and it is thus easy to terminate the slug injection by reading the injection pressure level before it reaches the reservoir damage pressure limit. While, in a continuous injection process, a stabilized increase in reservoir pressure is observed as long as injection is in progress, in contrast to during slug-wise injection. On average 28333 sm^3 of gas was injected over 8 hours during a slug injection process, as given in the history data, and was ceased for two days before the start of the next slug. Gas was continuously injected at a rate of 8151 sm^3/day including one slug (28333 sm^3 of gas in 8 hours) at the end of each year to compare the injection pressure trend in slug + continuous strategy with a pure slug injection plan. A slug that was part of a continuous + slug injection strategy completely overlapped the slug of a pure slug injection plan as shown in Figure 5. This finding validated the implementation of continuous + slug injection scheme which will significantly save the simulation time and disk space compared to slug injection strategy.

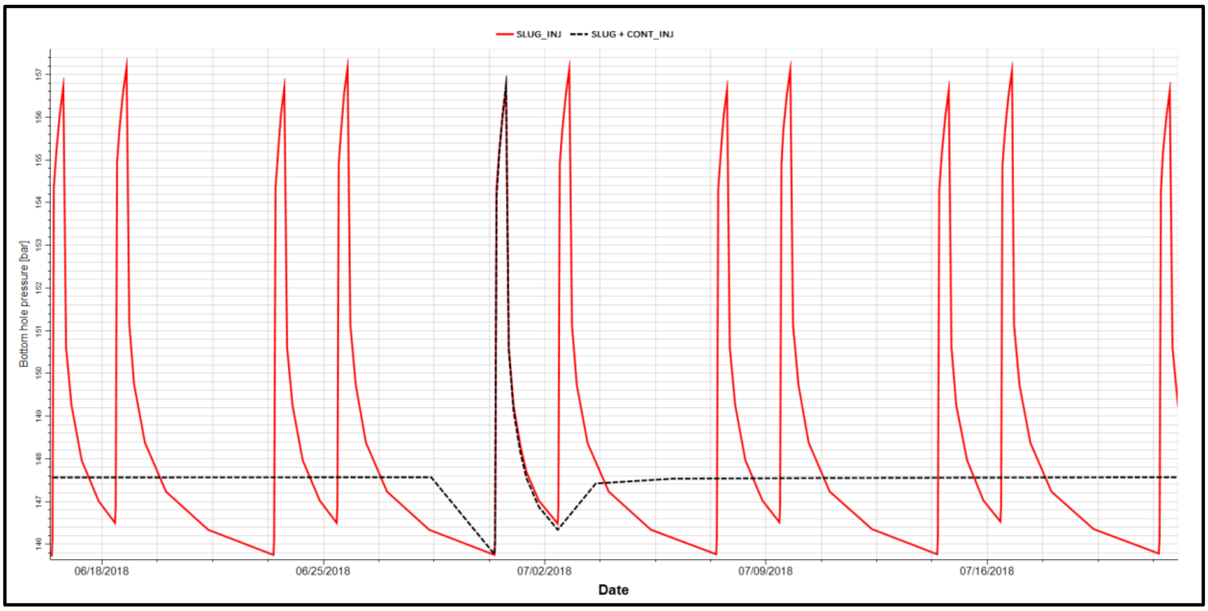

Figure 5. Comparison of slug injection pressure of pure slug injection plan with slug + continuous injection scheme.

The plot of water and CO_2 WAG-type slug injection is shown in Figure 6. Each predicted strategy starts from the historical injection period and then continues for 30 years or more forward in time. It can be seen that reservoir pressure rose from 143 to 149 bar during the brine and gas slug injections over 30 years. However, the injection pressure rose to 163 bars in the beginning (July 2017) and then gradually declined to 157 bar until April 2019 and then again steadily increased to 159 bar over the 30 years injection time. This pressure behaviour shows the greater ease of the gas flow with time in a homogeneous reservoir, which could be associated with increasing gas relative permeability due to an increase in gas saturation. Build-up and reservoir pressures for the water phase are slightly greater than the gas phase because water is more viscous and denser than CO_2. The WAG process started with water injection in the historical data, possibly to make sure the gas would flow away from the well into reservoir. It was found that the simulation time for the pure slug injection strategy was too lengthy (> 24 hrs) and it required 240 GB space on the hard disk, which limited its potential use for sensitivity analysis. Therefore, a pure slug injection strategy was replaced with a continuous + slug injection scheme which included continuous injection followed by one slug at the end of each year to make sure that the injection pressure follows the same trend as observed in pure slug injection plan.

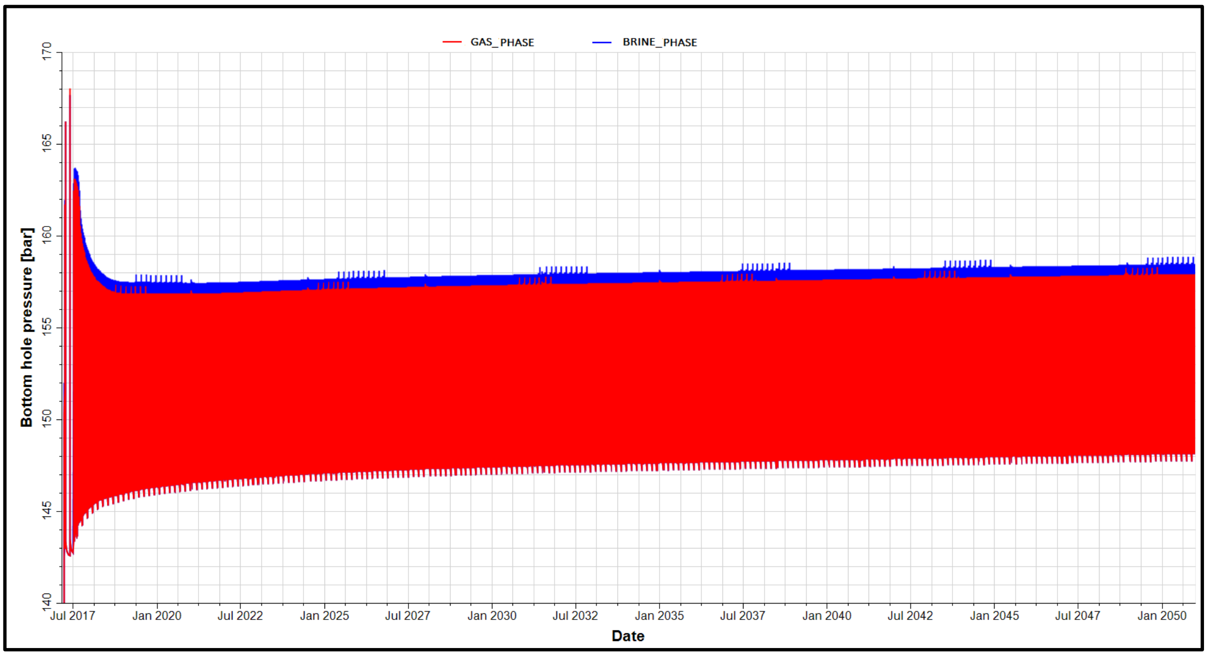

Figure 6. Injection and bottom-hole reservoir pressures during water alternating gas slug injections in gas and brine injection wells for 30 years.

In the continuous + slug injection strategy, equal volumes of gas and brine were injected over the course of each year as were injected during the pure slug injection process. The conversion of slug volumes into per day injection rate has already been explained above. A plot of continuous + slug injections for 80 years is shown in Figure 7. It can be seen that reservoir pressure rose from 143 to 149 bar during the 30 years of injection, which is the same as for the pure slug injection strategy. On continuing the injection of brine and gas, the reservoir pressure increased by 2 more bars over the next 50 years after 2050. However, the injection pressure gradually elevated to 159 bars over 80 years. The simulation time for the continuous + slug injection strategy is significantly shorter than the slug injection plan. The trends in the build-up and reservoir pressure matched with the pressures for the pure slug injection strategy. It can be seen from Figure 8 that the lateral movement of the CO_2 plume within the homogeneous reservoir model was mainly in an east-west direction, rather than a north-south direction, which respected the in-situ fracture density. In the homogeneous base case, CO_2 was injected at 100% water saturation and most of the CO_2 migrated to the top of the structure as a free gas. The direction of the CO_2 migration in the vertical plane is depicted in Figure 9, which shows a slice of reservoir grid in the Y direction. In the homogeneous model, the k_v/k_h ratio was equal to 0.1; at this permeability ratio the migration of CO_2 is more in a vertical direction compared to a lateral direction. This migration direction will trigger the hydrodynamic trapping mechanism in which CO_2 traps as a separate phase beneath an impermeable cap rock.

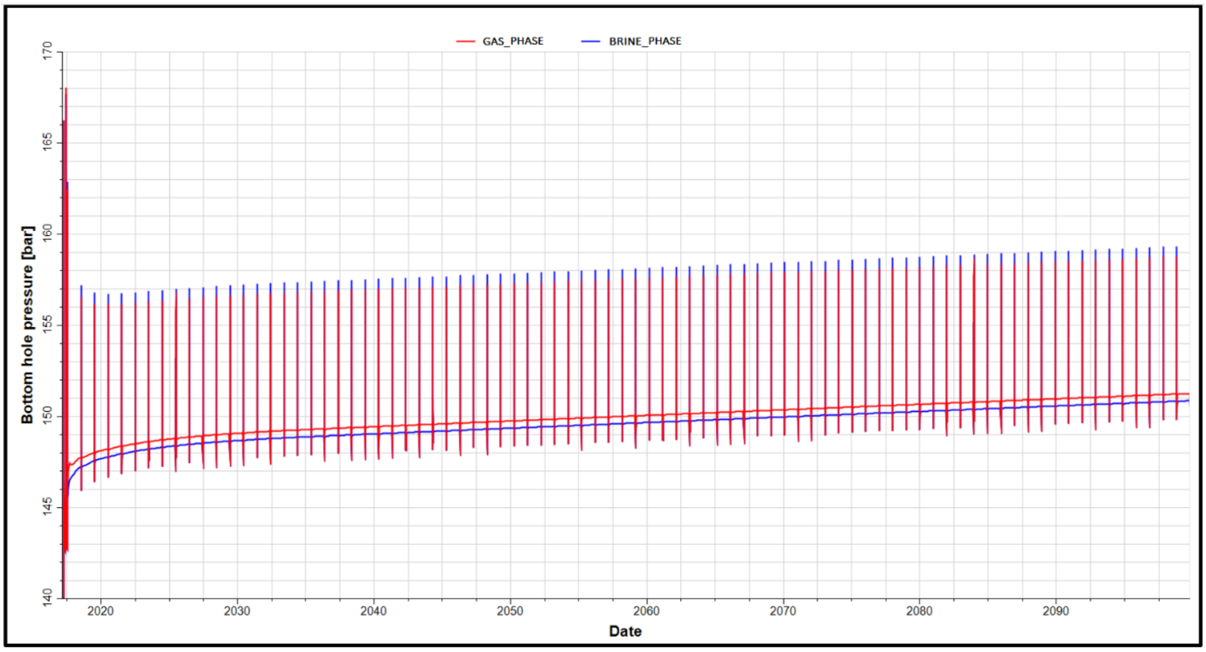

Figure 7. Build up and bottom-hole reservoir pressures during slug + continuous injection of water alternating gas over 80 years.

4.1 Injected Volumes and Reservoir Pressure

In a sensitivity study brine and gas were injected at a constant rate of 6 sm^3/day and 8151 sm^3/day respectively. At the end of each year the constant rate was replaced with a slug injection. In each slug 200 sm^3 of brine was injected for 2 hours and 28333 sm^3 of CO_2 was injected for 8 hours. The injected slug volumes were based on the averaged slug volumes given in the historical data. The cumulative volume of gas that was injected in reservoir over 100 years' time is given in Figure 10. However, when the gas injection rate was doubled (16370 sm^3/day) or tripled (24556 sm^3/day) compared to the base_case, the reservoir shut in pressure increased from 150 bar, to 160 bar or 165 bars, respectively, over 100 years injection time. The water injection rate was constant in these three simulated cases. However, the build-up pressure in double and triple gas injection cases was less than the reservoir fracture pressure, which is 200 bar, as measured by Dios et al. [(13)] Therefore, there is still capacity to inject the gas at a higher rate into the reservoir before it reaches the reservoir fracture pressure. The difference in reservoir pressure between the different cases was continuously growing with time, as it can be seen in Figure 11. The difference in reservoir pressure between the base case and the doubled gas injection case would be approximately 4 bar in 2020 and it increased to 8 bar by 2120. Similarly, the difference in reservoir pressure between base case and the triple gas injection case would be approximately 6 bar in 2020 and it would have increased to 10 bar by 2120. The trend of pressure gradient was quite sharp in the beginning and it started declining as long as the gas was injected. The shut-in pressure gradient became sharp as the gas injection rate was increased.

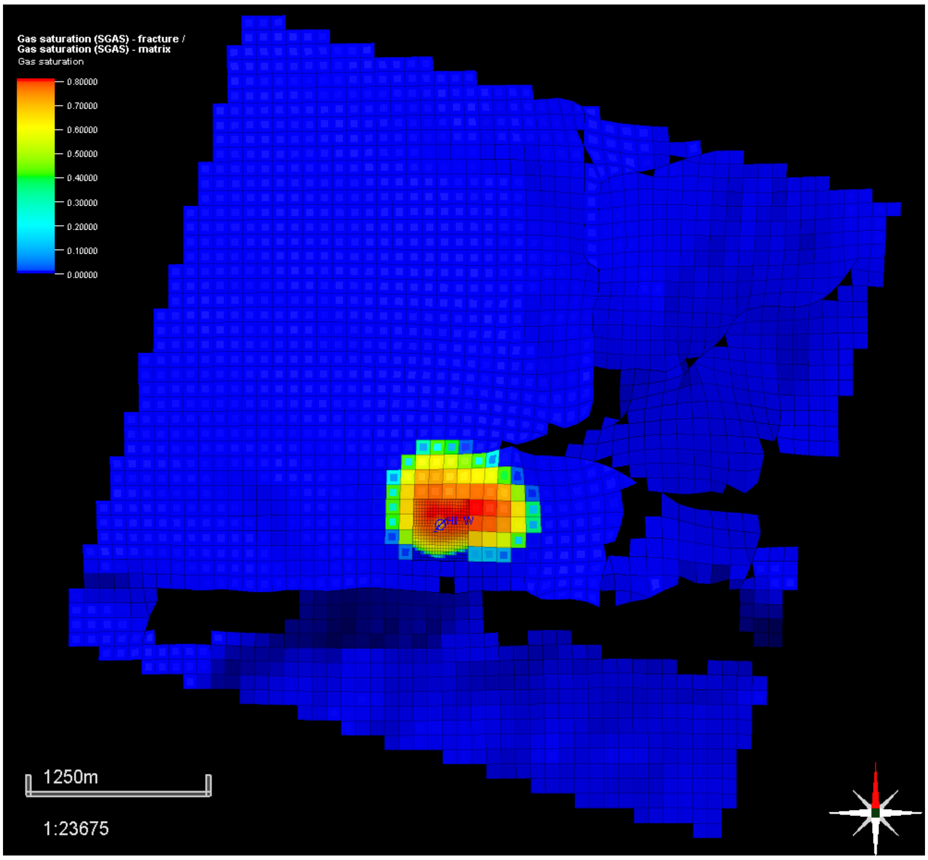

Figure 8. Migration extent of the CO_2 plume in horizontal direction during water alternating gas injection at a rate of 6 and 8151 sm^3/day respectively for 80 years.

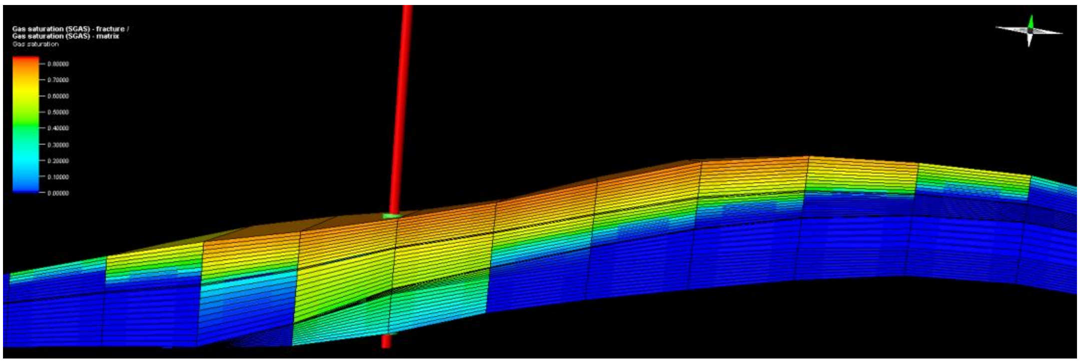

Figure 9. Migration extent of the CO_2 plume in vertical direction during water alternating gas injection at a rate of 6 and 8151 sm^3/day respectively for 80 years. The slice of the reservoir grid is taken in the Y direction.

5 Simulation Results for Heterogeneous Model

In this study, several heterogeneous models were simulated by changing the reservoir porosity, vertical to horizontal permeability ratio, and matrix and fracture permeabilities in different directions. The heterogeneous models were characterised into four categories, the first is related to variation in matrix and fracture permeabilities in different directions to investigate its impact on CO_2 plume migration. In the second type, the reservoir porosity was changed to observe how it affects the reservoir storage capacity and migration of CO_2 plume. In the third type, the vertical-to-horizontal permeability ratio was altered, and, in the final type, stochastic permeability models were created using a sequential Gaussian simulation method [14]. The variation in reservoir parameters for the first three types of heterogeneous models, with respect to finally matched (base_case) simulated case, are shown in Table 2.

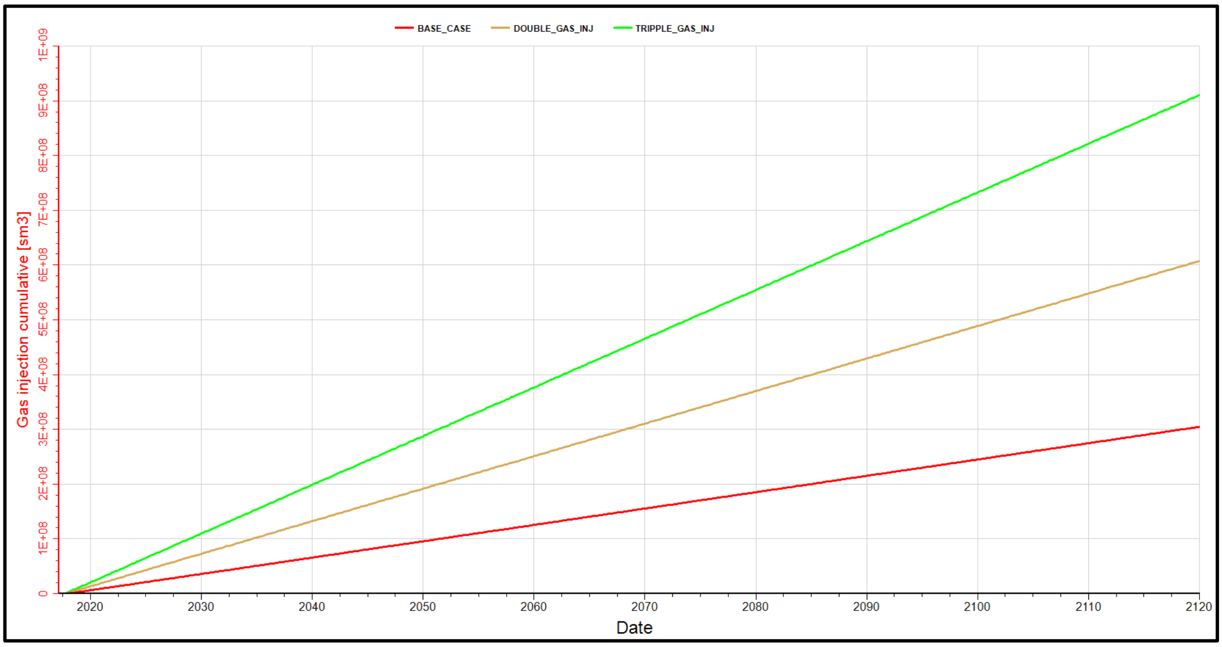

Figure 10. Cumulative injected volume of gas over 100 years' time. The green and brown lines show the cumulative injected volume of gas when the gas injection rate was triple and double respectively compared to the base_case.

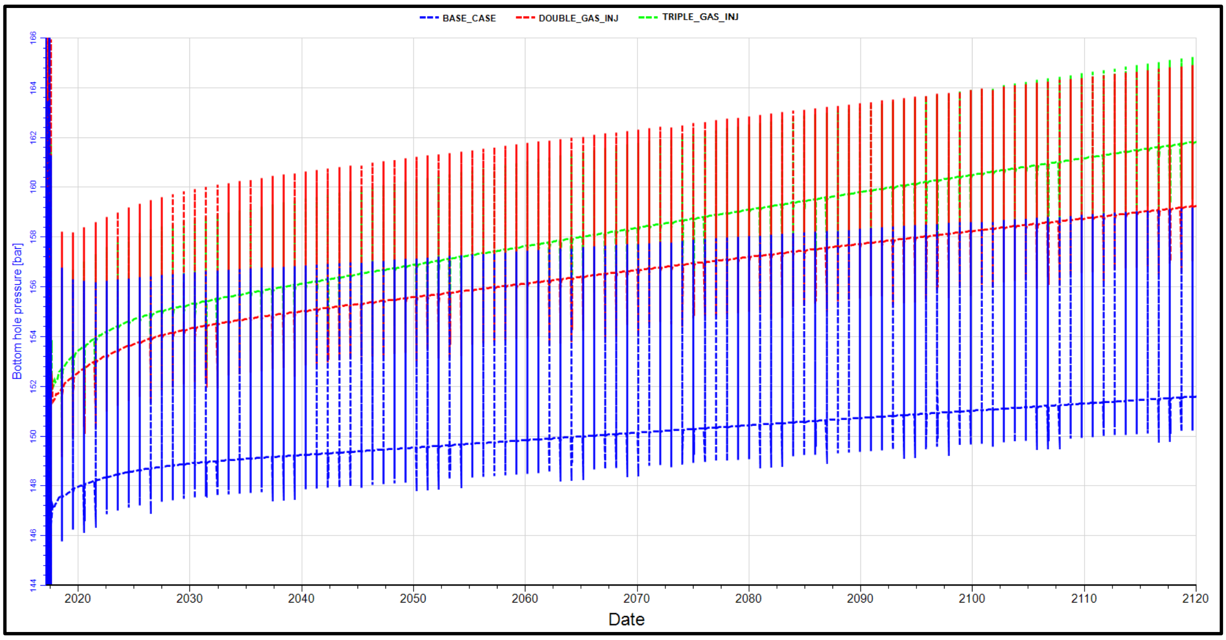

Figure 11. Comparison of injection and reservoir pressures of base case with double and triple gas injection rate cases over 100 years of gas injection.

Table 2. The percent change in reservoir parameters with respect to finally matched case (base_case) in sensitivity runs.

Cases	Km_X	Km_Y	Km_Z	ϕ_m	Kf_X	Kf_Y	Kf_Z
#	%	%	%	%	%	%	%
BASE_1	-83	-88	-75	0	0	0	0
BASE_2	33	-88	-75	0	0	0	0
BASE_3	-83	0	-75	0	0	0	0
BASE_4	-83	-88	1900	0	0	0	0
BASE_5	0	0	900	0	0	0	0
BASE_6	0	0	1900	0	0	0	0
BASE_7	0	0	0	-50	0	0	0
BASE_8	0	0	0	50	0	0	0
BASE_9	0	0	0	150	0	0	0
BASE_10	0	0	0	0	100	0	0
BASE_11	0	0	0	0	0	97	0
BASE_12	0	0	0	0	0	0	97
BASE_13	33	-25	0	0	29	-23	0
BASE_14	0	0	-50	0	29	0	-23
BASE_15	0	0	0	0	0	0	-95
BASE_16	0	0	100	0	0	0	-90
BASE_17	0	0	300	0	0	0	-80
BASE_18	0	0	900	0	0	0	-50
BASE_19	0	0	1900	0	0	0	0
BASE_46	100	0	0	0	0	0	0
BASE_47	0	97	0	0	0	0	0
BASE_48	0	0	97	0	0	0	0

5.1 Effect of Permeability Variation

At first, the simulated case matrix permeability was set to 0.5 mD in the horizontal direction and 0.05 mD in the vertical direction, as distributed in the original geological model. The other reservoir parameters were kept constant as given in Table 1. The percent change variation in porosity, matrix and fracture permeabilities with respect to the base_case is given in Table 2. The reservoir and injection pressures increased 2 to 6 bars respectively compared to reservoir and injection pressures of final history matched case (base_case) during gas slug injections over 30 years. It can be seen from the data given in Figure 12 that these pressures continuously increased with time as long as gas was being injected.

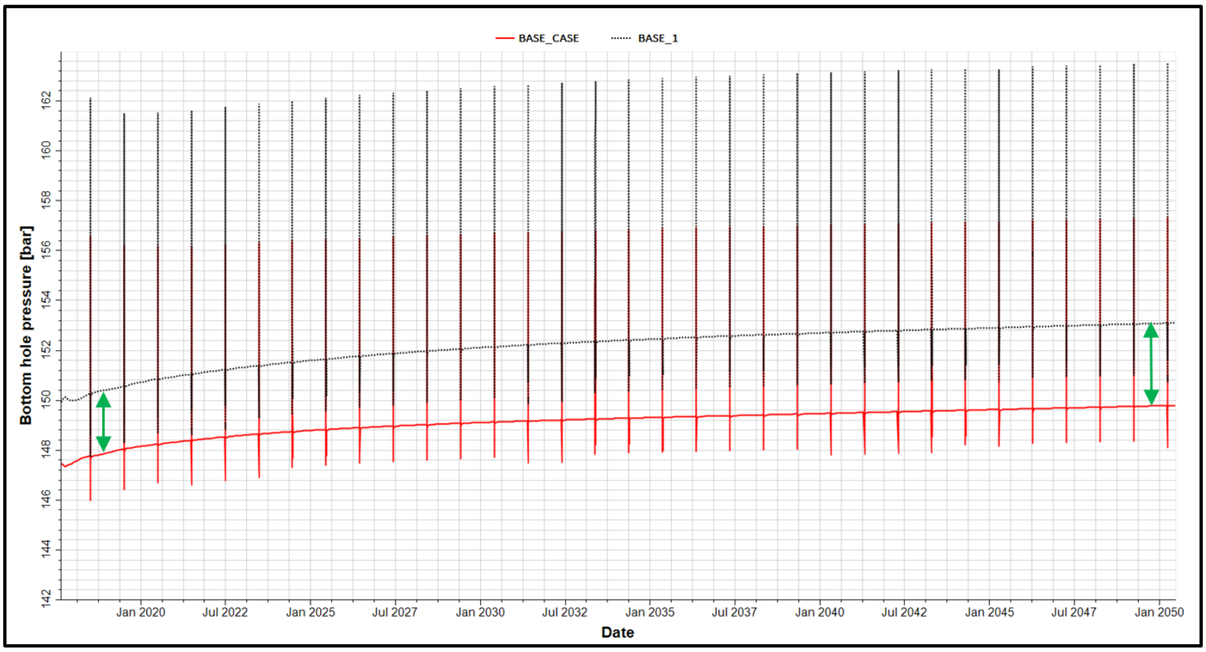

Figure 12. Comparison of injection and reservoir pressures in validated base_case and base_1 during gas injection for 30 years.

In the sensitivity runs from Base_1 to Base_4, the matrix permeability was changed in the X, Y and Z directions compared to the base_case. The percent changes in matrix permeability in each respective direction for these four cases compared to the base_case is given in Table 2. A significant increase in matrix permeability in the Z-direction slightly decreased the build-up and reservoir pressures, as can be seen by comparing case base_1 with base_4 in Figure 13. However, the pressure response was different for the matrix permeability variation in the XY direction compared to the base_case, as can be observed by comparing case base_2 with base_3. By decreasing the permeability either in the X or Y directions, the reservoir and injection pressures increased 2 to 3 bars compared to the base case over 30 years injection. Moreover, pressure behaviour was different when permeability was increased in the X direction compared to the Y direction, since pressure decreased less than half bar in the beginning and then slightly increased at the end compared to the case in which Y direction permeability was increased by the same amount. The CO_2 plume movement direction significantly changed as the matrix permeability was increased substantially in one particular direction compared to the other directions. The CO_2 plume migrated more in Y-direction (E-W) compared to X-direction (N-S) when matrix permeability increased in east-west direction and vice versa. This E-W and N-S trending of CO_2 plume movement can be seen in upper and lower part of the Figure 14 respectively.

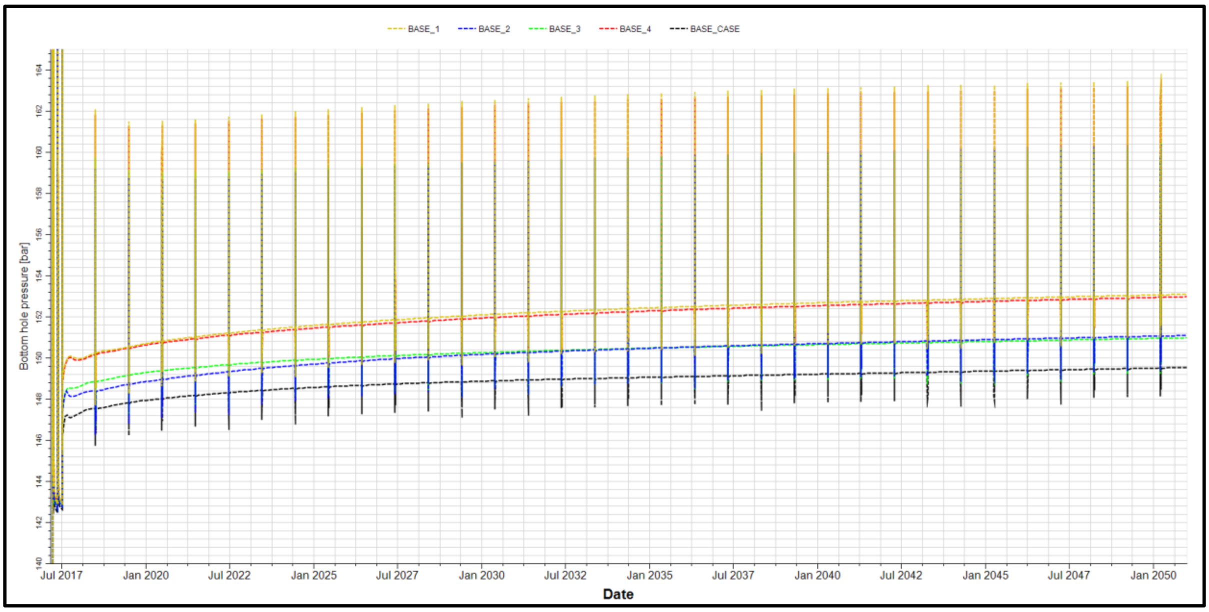

Figure 13. Build up and bottom-hole reservoir pressures by changing matrix permeability in direction and value during gas slugs' injection for 30 years. The matrix permeability in X, Y and Z direction was increased from 0.5 mD to 4 mD one by one in cases base_2 to base_4 and compared with case base_1 in which permeability is 0.5 mD in XY direction and 0.05 mD in Z direction.

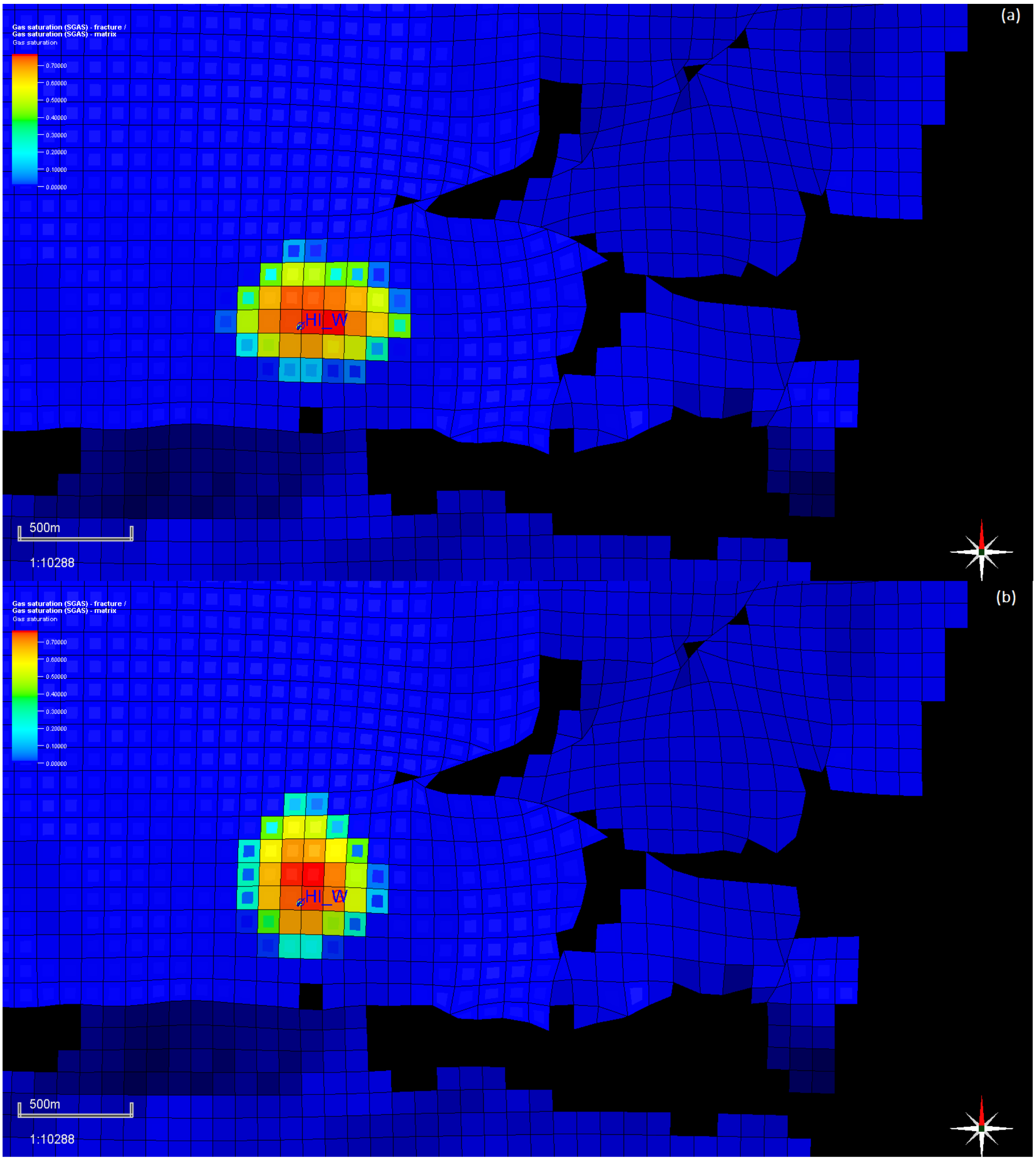

Figure 14. The part (a) shows E-W and part (b) shows N-S movement of CO_2 plume when matrix permeability increased in X and Y direction respectively in 30 years of gas injection.

In the model sensitivity runs Base_10 to Base_12, the fracture permeability was changed in the X, Y and Z directions one by one. The fracture permeability was increased two times more than the original fracture permeability that was used in the base_case. A two times increase in fracture permeability in the Z direction had no significant effect on build-up and reservoir pressure compared to the base case. However, the pressure response is slightly different for fracture permeability variation in the X and Y directions, as can be seen from Figure 15. By increasing the fracture permeability either in the X or Y direction, the reservoir and injection pressures reduced by 0.5 to 1 bar compared to the base_case after 30 years injection time.

Pressure behaviour is slightly different when fracture permeability increased in the X direction, as it decreased a little bit in the beginning, and, then, marginally increased at the end compared to the case base_11 in which Y permeability was changed by the same magnitude. A similar trend in pressure was observed when matrix permeability was changed in the same pattern but it was a bit pronounced in that case because the matrix permeability variation was 5 times greater compared to fracture permeability variation. The CO_2 plume migration direction clearly changed as the fracture permeability increased in X and Y directions, respectively. The CO_2 plume was migrating more in the Y-direction (E-W) compared to the X-direction (N-S) when fracture permeability increased in east-west direction than vice versa. The E-W and N-S CO_2 plume migration trend was similar as was observed during matrix permeability variations in same directions.

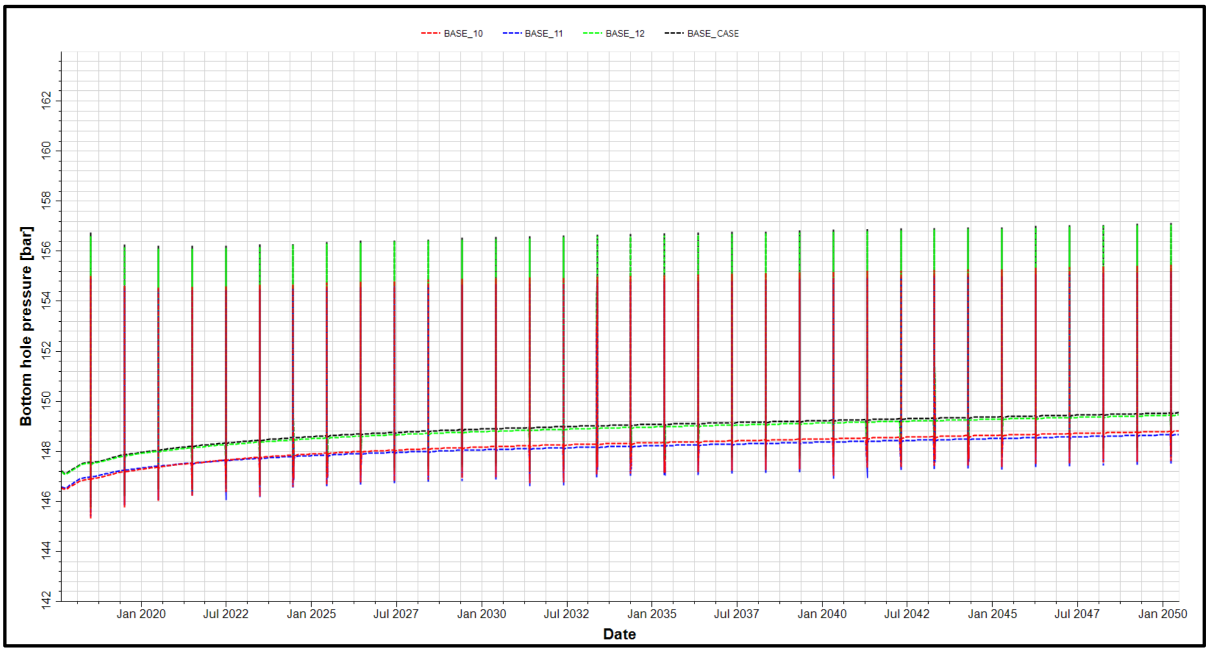

Figure 15. Build up and bottom-hole reservoir pressures by changing fracture permeability in X, Y and Z direction during gas slugs' injection for 30 years. The case base_10 shows change in fracture permeability in X-direction while base_11 and base_12 show change in fracture permeability in Y and Z direction respectively.

When the degree of matrix and fracture permeability change in the XY direction is similar the CO_2 plume migration distance from the injection well is similar. The spread of the plume can be seen in Figure 16 for when the change in matrix and fracture permeability in the X-direction was 2 times greater than the base_case. However, the same degree of matrix and fractures permeability change in the Z-direction did not produce identical results. It was observed that the CO_2 plume spread was a bit different when matrix and fracture permeability in Z direction was increased 0.97 times compared to the base_case and it can be seen in Figure 17. The plume spread was slightly broader in matrix case compared to the fracture case while the increase in permeability in both cases was 97% compared to the base case.

The reservoir pressure response was different compared to CO_2 plume migration when the change in matrix and fractures permeability was similar compared to the base case. It was observed that the reservoir and build-up pressures rose 0.5 bar more in case of an increase in the fractures permeability compared to an identical doubling in the matrix permeability. The difference of pressure (0.5 bar) stay constant over the whole period of injection in both cases and it can be seen in Figure 18.

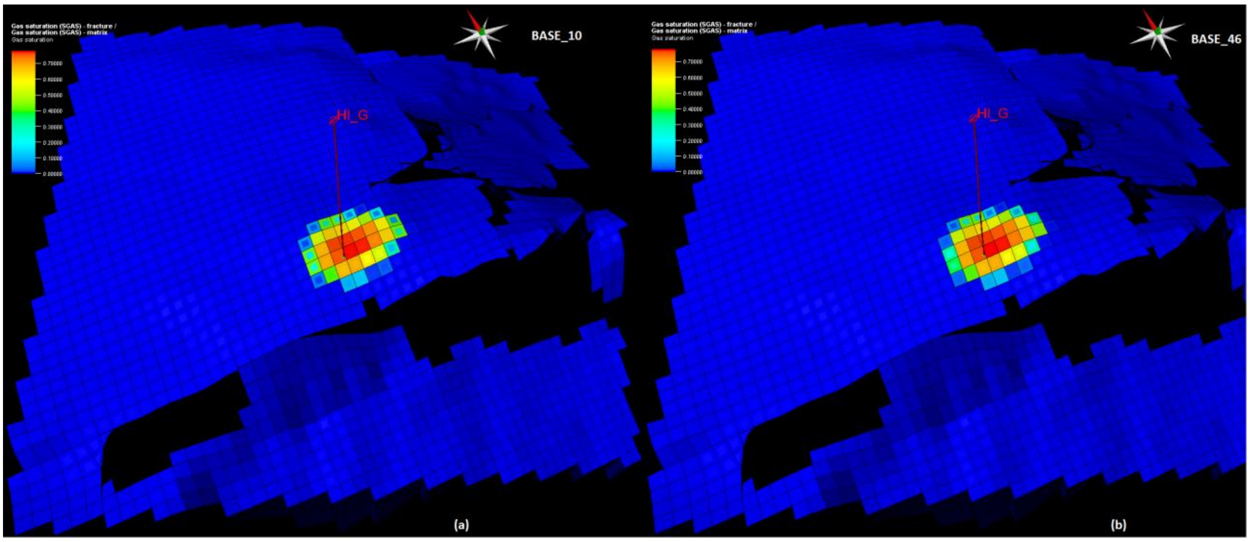

Figure 16. Comparison of CO_2 plume migration from injection well when change in matrix and fracture permeability in X direction is 100% compared to the base_case in part (a) and part (b) respectively. The CO_2 plume spread in both cases is identical.

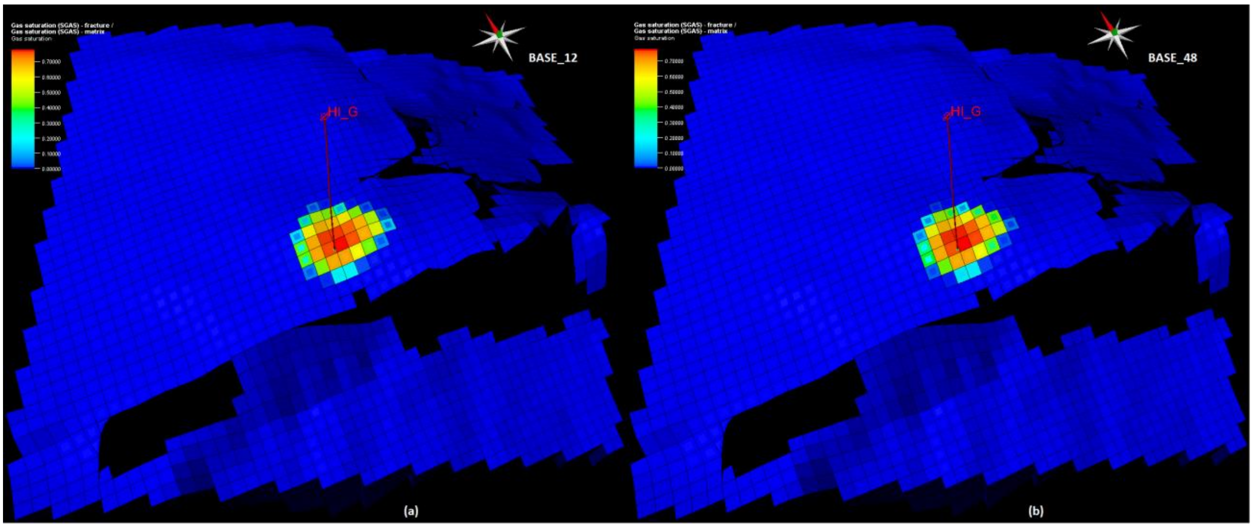

Figure 17. Comparison of CO_2 plume migration from injection well when change in matrix and fracture permeability in Z direction is 97% compared to the base_case in part (a) and part (b) respectively. The CO_2 plume spread in both cases is different, its spread is a bit larger in part (a) compared to part (b).

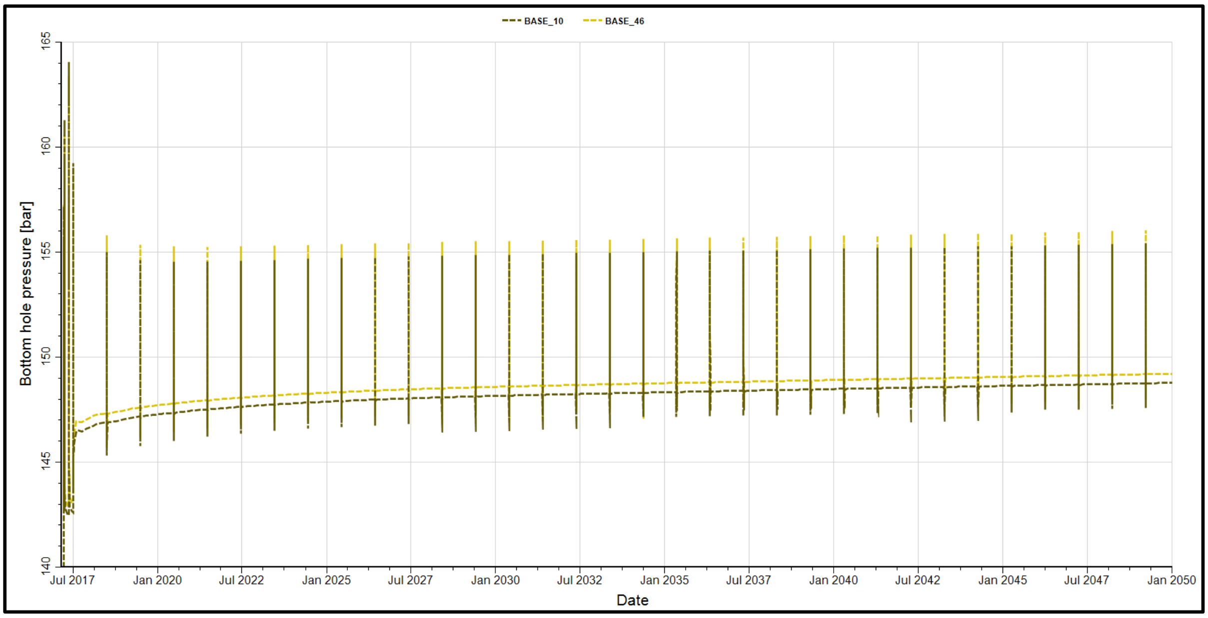

Figure 18. Comparison of build-up and bottom-hole reservoir pressures at 100% increase in matrix and fracture permeability in X direction compared to base_case over 30 years of gas injection. The case base_10 shows change in matrix permeability in Y-direction while base_46 shows same degree of fracture permeability change in Y direction respectively.

5.2 Effect of Porosity Variation

The storage capacity of the reservoir depends upon matrix porosity and it changes accordingly as matrix porosity changes. It can be seen from Figure 19 that, while the same amount of CO_2 was injected for the same period of time, the migration distance of the CO_2 plume from the injection well was significantly different when porosity was different. When the porosity of the reservoir was half of the original porosity as defined in the geological model, the CO_2 plume moved to a larger distance compared to the case when reservoir porosity was 2.5 times greater than the porosity as defined in the original geological model and this behaviour is depicted in upper and lower part of Figure 14, respectively. However, the effect of change in matrix porosity on reservoir and injection pressures is not as significant as that on the movement of CO_2 plume as can be seen in Figure 20. The change in pressure is related to ease of gas flow which depends on reservoir permeability and gas saturation more than the porosity. Therefore, reservoir and injection pressures did not change significantly by changing the matrix porosity. CO_2 plume travelled a larger distance from the injection well when porosity was decreased compared to the case in which matrix porosity was increased.

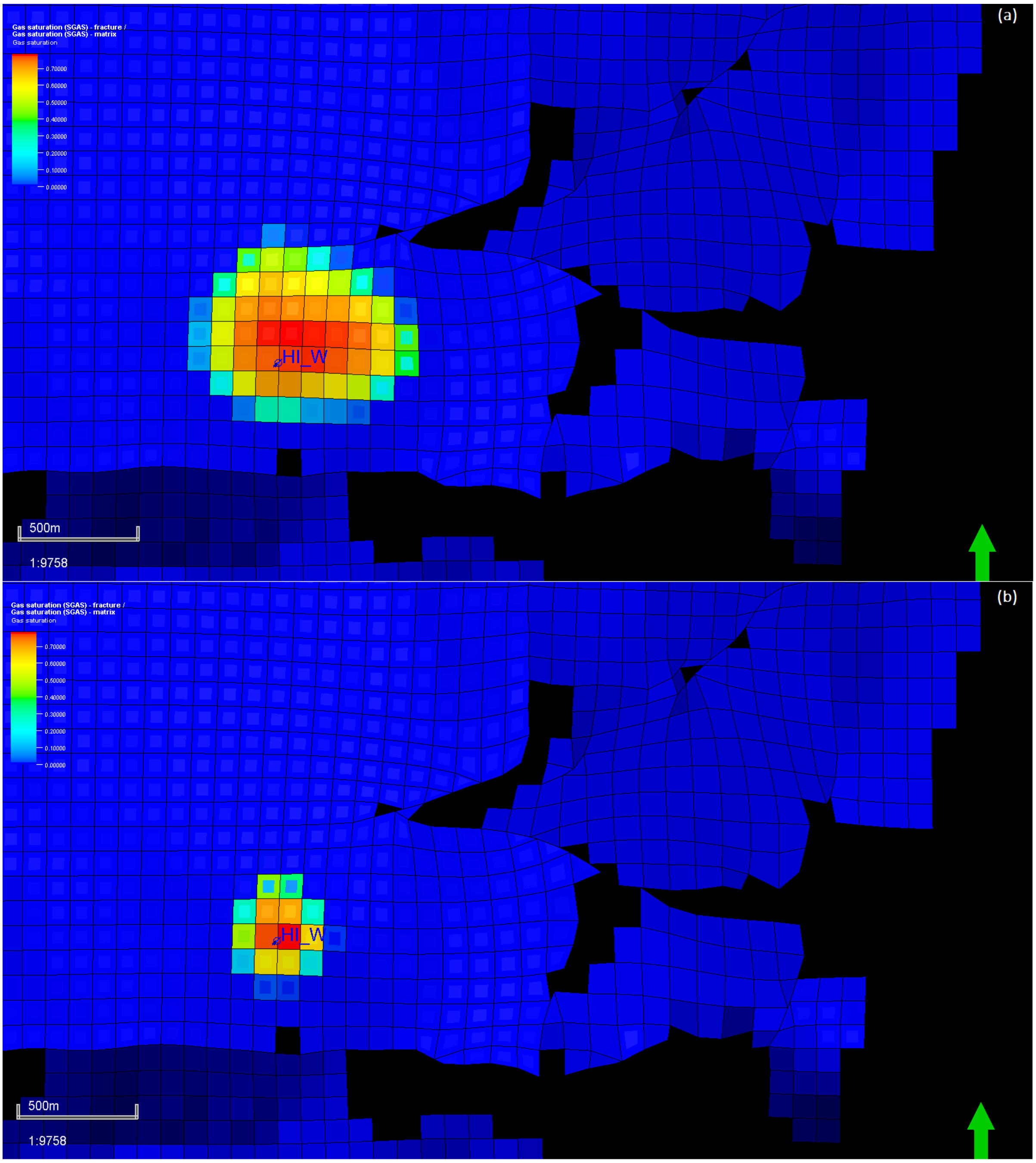

Figure 19. Movement of CO_2 plume when reservoir porosity is 0.5 in part (a) and 2.5 in part (b) times to the original porosity of base_case in top and bottom part respectively after 30 years of gas injection.

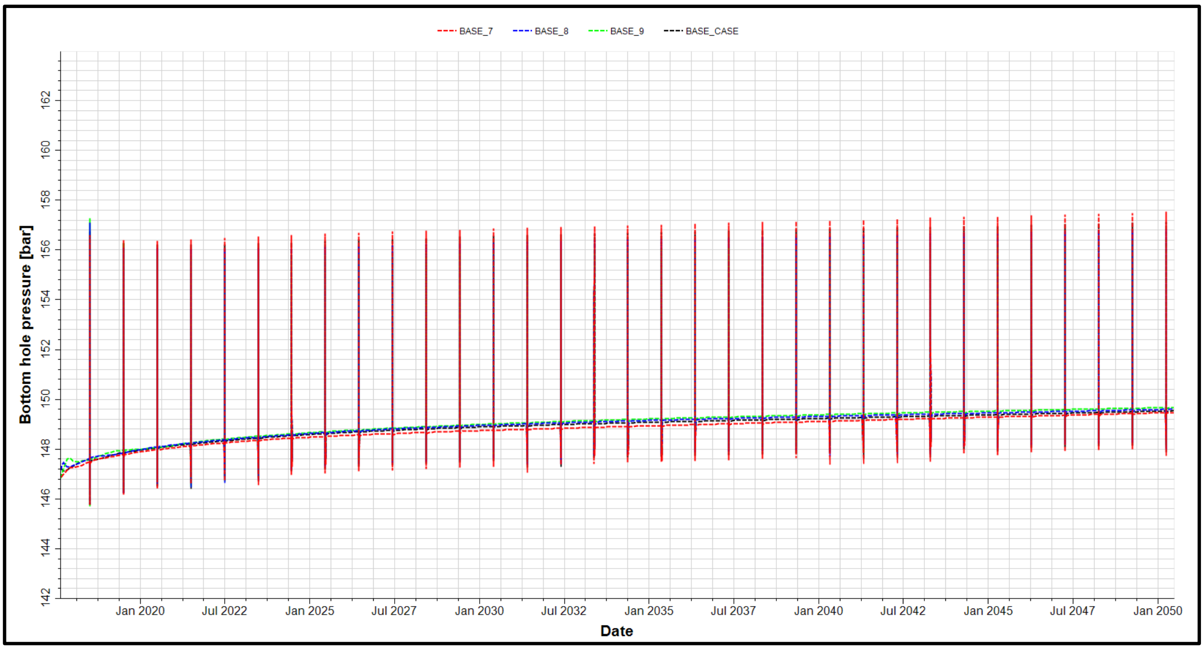

Figure 20. The response of build-up and reservoir pressures by changing matrix porosity during gas injection for 30 years.

5.3 Effect of k_v/k_h Ratio

An increase in kv/kh ratio increased the rate of vertical movement of gas during injection phase. Therefore, the amount of carbon dioxide which was immobilized due to solubility trapping (CO_2 stores in the solution depending on brine salinity, temperature and pressure) may increase when kv/kh increased as described by Ghanbari et al. [(15)]. The lateral migration of CO_2 became dominant as the kv/kh ratio decreased and ultimately there might be a risk of possible gas leakage through the aquifer boundaries. Lateral migration of CO_2 plume can be seen in Figure 21 when vertical to horizontal permeability ratios were decreased from 1 to 0.05 for a similar period of time at same injection rate. However, when kv/kh ratio was equal to 1 the gas plume was mainly migrating towards the top of the structure and accumulating under the cap rock. The accumulation of gas under the seal rock is known as hydrodynamic trapping in which CO_2 is stored as a free gas phase. However, build-up and reservoir pressures did not significantly change when fracture and matrix vertical permeabilities varied from 0% to 95% of the horizontal permeability. The difference in build-up and reservoir pressures was less than half a bar after 30 years of gas injection when kv/kh was 1 as can be seen in Figure 22.

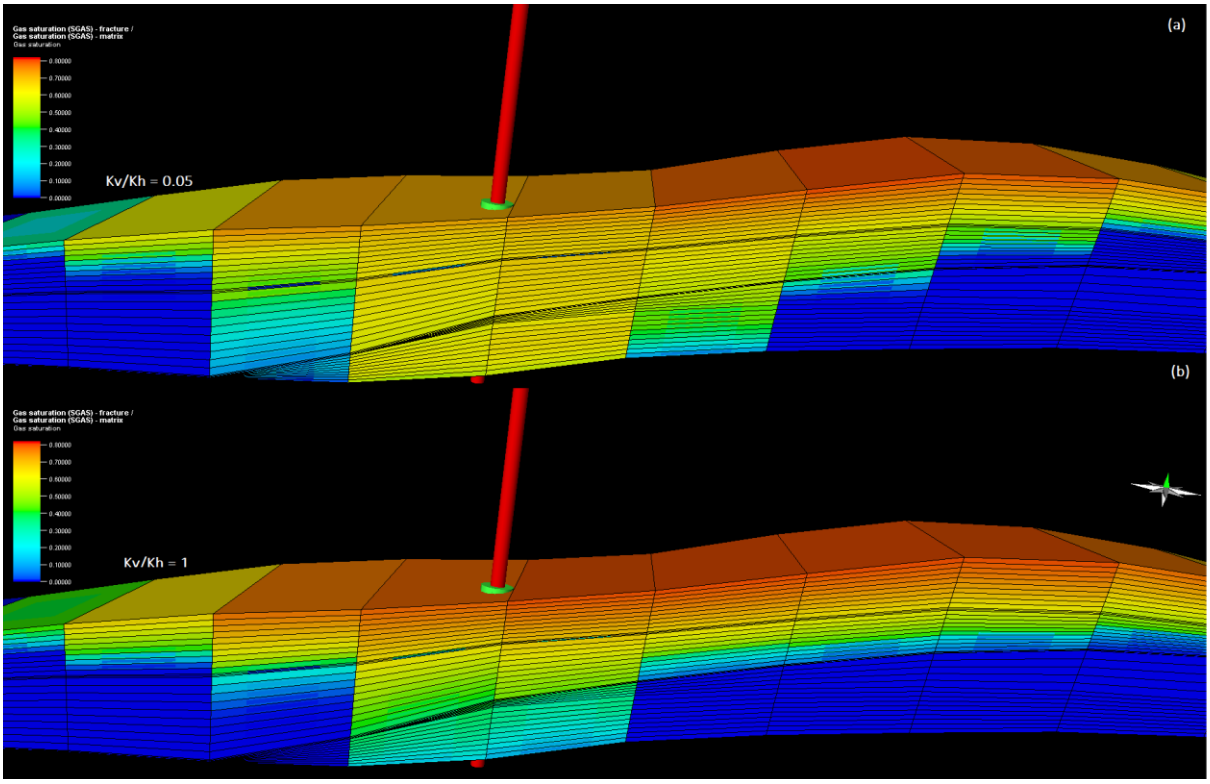

Figure 21. Movement of CO_2 plume in horizontal and vertical direction when Kv/Kh increased from 0.5 to 1.05 in part (a) and (b) respectively during gas injection for 30 years. The displayed grid cell slice of the reservoir was taken in Y-direction.

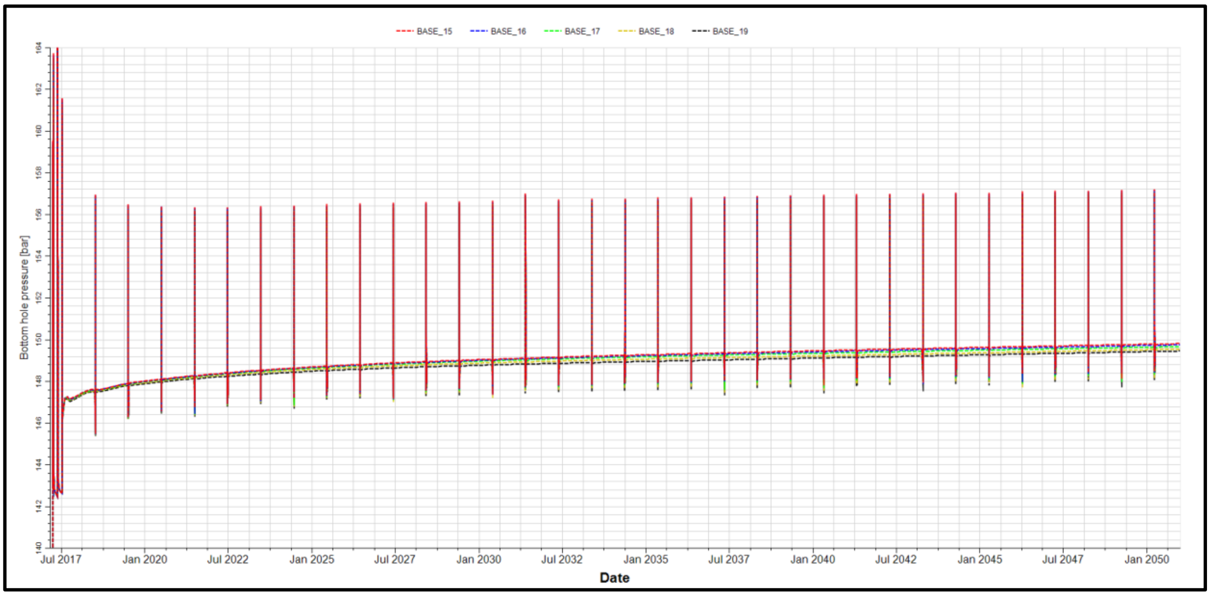

Figure 22. Simulated build-up and reservoir pressure limits when kv/kh was gradually changed for matrix and fractures during gas injection for 30 years. Vertical permeability was decreased from 0% to 95% of horizontal permeability for fractures and matrix in cases base_15 to base_19 compared to base_case.

5.4 Effect of Random Permeability Distribution

The effect of random matrix permeability variation on the flow of the CO_2 plume, and on reservoir pressure, during a long-term injection strategy was investigated. Fifteen permeability realizations were generated using a sequential Gaussian simulation method with standard Gaussian distribution. The permeability distribution range was selected from 0.5 md to 4 md in all the six zones of the reservoir as shown in Table 3. Realizations were produced using the Latin-hyper cube sampling technique with a Monte-Carlo sampling method. In each realization a different value of matrix permeability was assigned to each zone in the uncertainty and optimisation workflow process in Petrel. Therefore, the change in matrix permeability in each realization produced a different kind of pressure response as shown in Figure 23. All of the six zones of the reservoir comprise a different number of layers and in the random permeability distribution process all layers of a zone have the same permeability, which is different from the layers of other reservoir zones. Movement of the CO_2 plume was different in each realization and depended on the assigned permeability value to each layer. The maximum increment in reservoir pressure compared to base case was 13 bar in 100 years injection time.

Table 3. Range of permeability distribution in Sequential Gaussian Simulation (SGS) method for different reservoir zones.

Sopena Reservoir Zones	Matrix Permeability (mD)		
	Base value	Min	Max
Upper Calcareous	0.6	0.5	4
Upper Baffle Calcareous	0.6	0.5	4
Middle Calcareous	0.6	0.5	4
Lower Baffel Calcareous	0.6	0.5	4
Lower Calcareous	0.6	0.5	4
Dolomitic	0.6	0.5	4

6 Reservoir Storage Capacity and Heterogeneity

This section describes the impact of geological heterogeneities on reservoir storage capacity. It provides an insight of the CO_2 plume migration and trapping in different heterogeneous settings of the reservoir. The geological models that used to investigate the reservoir storage capacity were generated by changing the matrix permeability. The CO_2 is being injected at constant injection rate instead of constant pressure. Therefore, reservoir storage capacity is derived from change in reservoir pressure by injecting a similar volume of gas over the same period of time into different heterogeneous models. The range of matrix permeability distribution in different zones of the reservoir in 15 simulated models is given in Table 4.

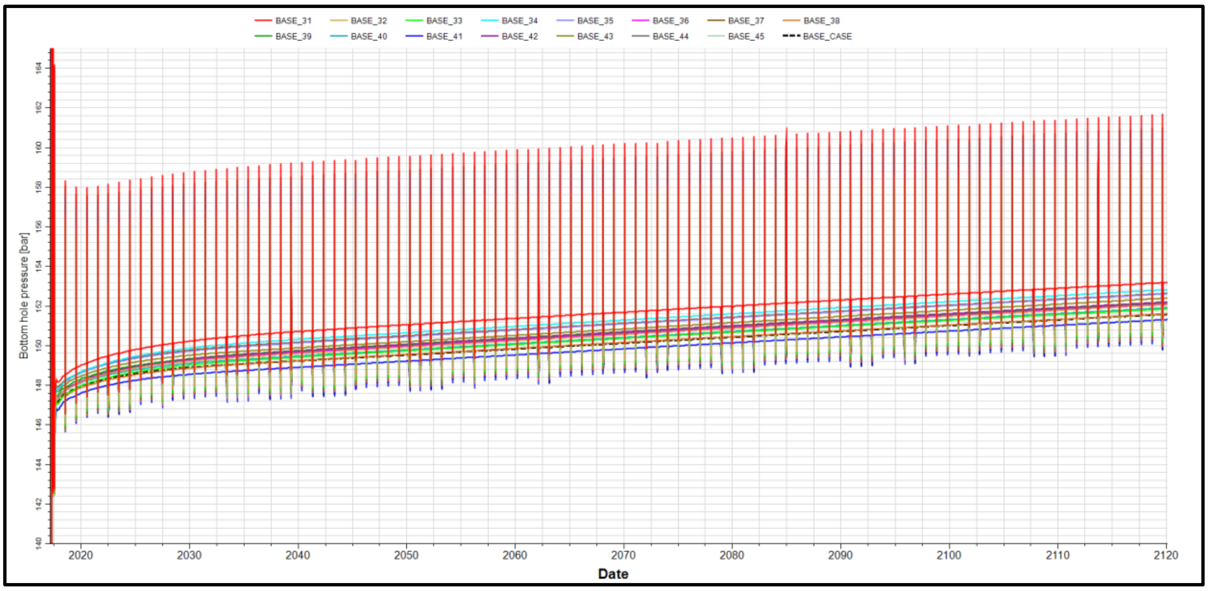

Figure 23. Simulated build-up and reservoir pressure responses in randomly permeability distributed cases during gas injection for 100 years. Reservoir pressure varied from 3 to 5 bar among the realizations.

Table 4. The range of permeability (mD) distribution in different zones of the reservoir in each simulated case.

Simulated	Upper Calcareous		Upper Baffle Calcareous		Middle Calcareous		Lower Baffel Calcareous		Lower Calcareous		Dolomitic	
Cases	Start	End	Start	End	Start	End	Start	End	Start	End	Start	End
BASE_31	3.004492	1.014975	3.036872	1.152852	2.846294	2.465739	1.714228	0.944115	2.300272	0.567117	2.237465	1.233711
BASE_32	1.071123	1.539441	3.27108	3.269109	1.47798	2.762161	1.134859	1.170519	3.872127	2.826971	1.746908	3.32673
BASE_33	3.493976	1.817427	1.132408	3.439057	3.582648	3.377136	3.028354	2.63088	0.750491	1.866273	1.309213	3.746422
BASE_34	1.340189	2.201592	2.921219	1.583198	3.803306	0.855031	3.8221	2.554513	1.618239	0.790627	2.641594	2.777815
BASE_35	2.695669	0.615387	1.404951	0.745775	2.498435	2.883657	2.409341	3.986595	2.840237	2.956804	1.450411	1.664543
BASE_36	0.644088	3.225641	2.360201	3.839559	3.87093	1.905891	3.90619	3.692496	0.634752	1.25509	3.152078	2.617219
BASE_37	1.550187	2.82594	1.716738	1.72664	1.804662	1.542299	3.560484	0.797725	2.473451	2.263565	0.562182	0.816369
BASE_38	3.702451	3.711386	0.692806	3.658711	3.087684	3.654043	1.338875	1.287642	3.291797	1.909181	0.725641	1.147575
BASE_39	2.222581	1.244964	3.852526	1.524103	1.259758	3.977574	3.289991	3.615339	3.117405	3.25352	2.324236	0.504903
BASE_40	0.953055	3.414997	2.147175	1.20595	2.196267	2.078247	2.459944	2.884704	3.55932	3.331574	2.788202	1.431948
BASE_41	3.236771	3.558518	1.216465	0.525454	1.042683	3.207221	2.096235	1.897212	3.807856	2.762898	3.624519	3.860601
BASE_42	2.57954	2.306948	3.312374	2.962011	0.930725	2.25541	3.363144	3.451421	2.660292	0.888897	1.046	3.637086
BASE_43	2.898943	2.467571	1.810318	2.658898	3.161819	0.733604	1.004791	1.990563	1.433641	3.789233	2.007637	1.932392
BASE_44	1.521737	3.901677	2.680885	2.510767	1.939057	1.683978	0.731169	2.199589	1.834811	1.550983	2.50493	1.748505
BASE_45	1.950459	3.037834	3.574306	0.92845	3.414805	1.730816	2.825326	1.560377	1.340574	1.421646	3.972554	3.05267

In heterogeneous models, the reservoir pressure change is dependent on the permeability of the matrix and will vary across the models during constant injection of CO_2 for similar periods of time. The reservoir shut-in pressure versus cumulative CO_2 injection for different simulated cases compared to base case is shown in Figure 24. Although the coefficient of variation of permeability in these cases is less than 60% still the reservoir storage capacity is markedly different. It is obvious from the comparison of these cases with the base_case, except for base_41, if the reservoir matrix permeability decreases the storage capacity also decreases. In the base_case, the reservoir permeability is 2 mD throughout the reservoir in contrast with the heterogeneous cases. It was observed by Ling et al. [16] that an increase in permeability is linked to increase in pore connectivity in carbonate reservoirs. Therefore, it could be speculated that an increase in matrix permeability in simulated cases increased the porosity which actually stores the fluid in reservoir. In the beginning the reservoir pressure sharply increased for all the cases and then progressively decreased as more volume of CO_2 was injected. However, the storage capacity still varied from one model to the next. It was observed that, at similar pressure, the injected volume of CO_2 is different among the simulated cases. This shows that the reservoir storage capacity varies among the heterogeneous models. It can be seen that at 14800 kPa pressure the CO_2 injected volume for case base_41 is 7 times higher than the base_31 that means reservoir can store 7 times more volume of CO_2 to reach the same pressure. The CO_2 plume migration in the horizontal directions away from the injection well in cases base_31 and base_41 is shown in Figure 25. Similarly, the mobility of CO_2 across the different layers of the reservoir in cases base_31 and base_41 is shown in Figure 26. Although the migration of plume is not significantly different, the stored injected volume to reach the same reservoir pressure is considerably different in each case. When looking at the vertical gas migration, both of the models show the gas reaching the uppermost part of the reservoir and spreading out under the cap rock. However, the saturation of gas is different in same layers of both cases and depends on matrix permeability.

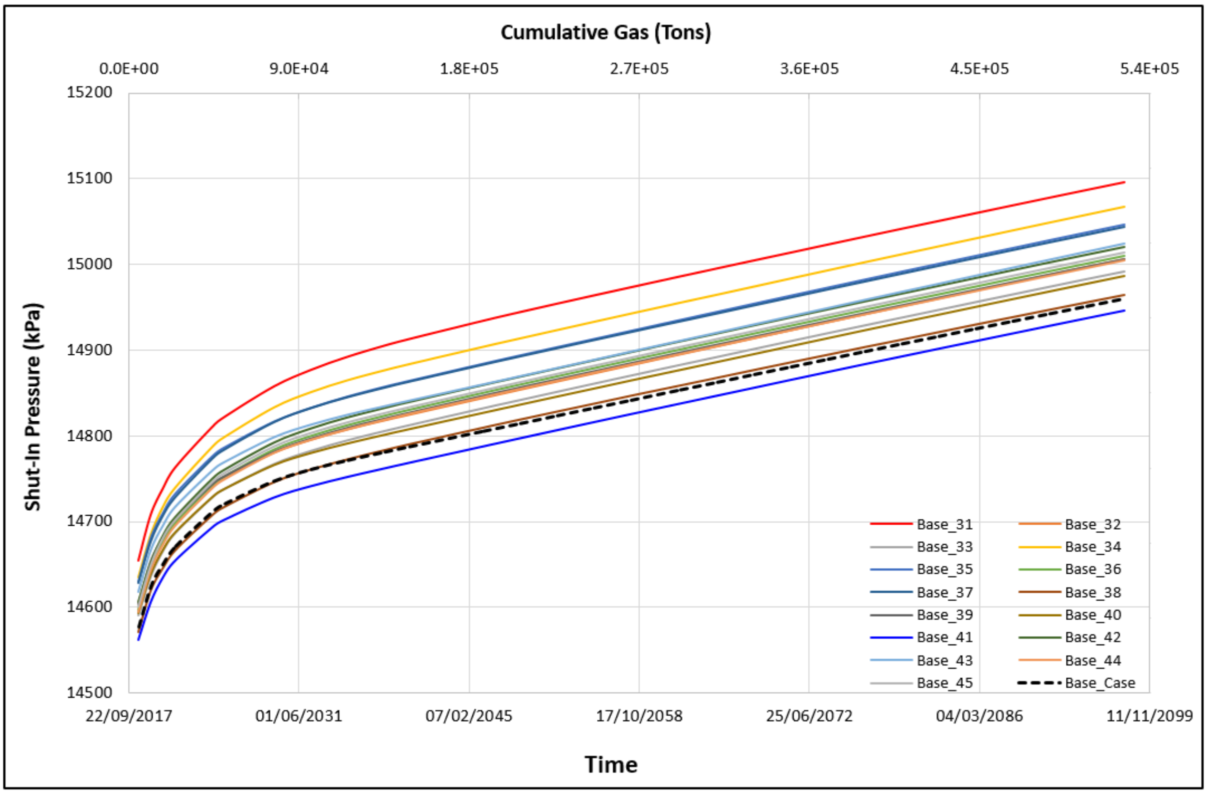

Figure 24. Reservoir shut-in pressure versus cumulative injection of CO_2 for similar time period. The heterogeneity of the simulated models based on the variation in matrix permeability.

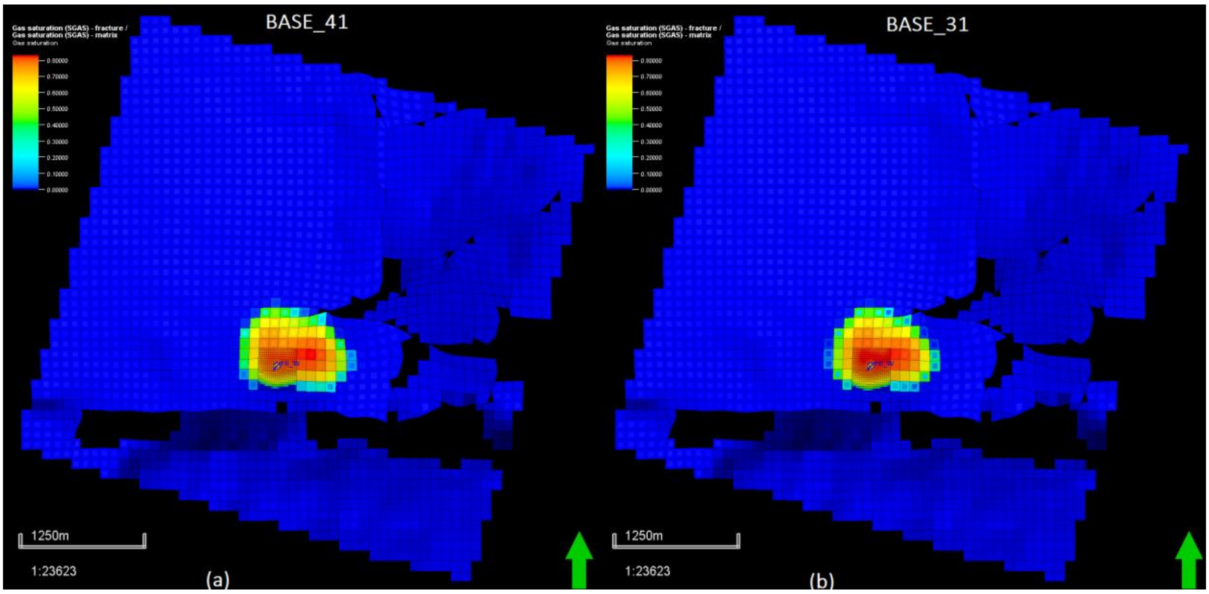

Figure 25. The part (a) shows the migration of CO_2 plume in base_41 and part (b) shows the migration of CO_2 plume in base_31 over 100 years of injection. The same volume of CO_2 is injected in both cases but the spread of plume is different in both cases.

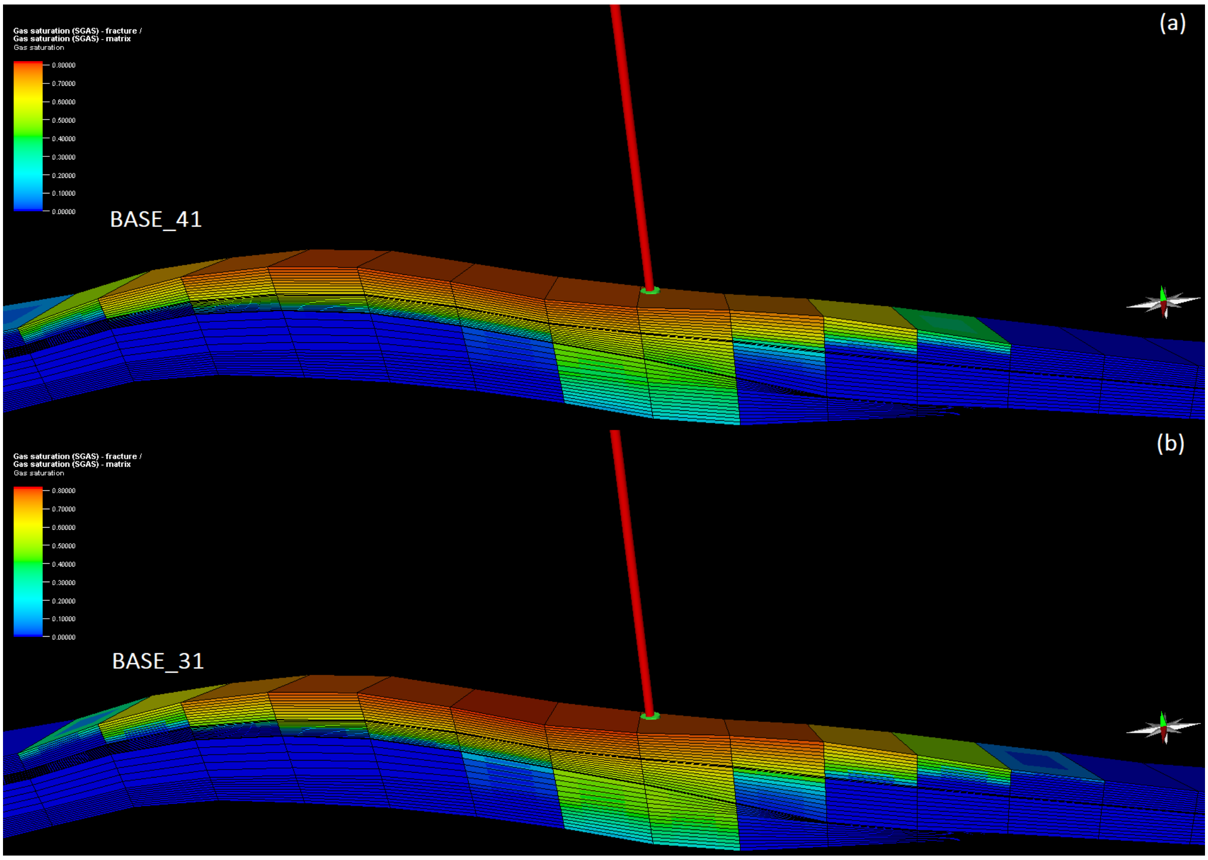

Figure 26. The part (a) shows the vertical movement of CO_2 plume in base_41 and part (b) shows the vertical movement of CO_2 plume in base_31 over 100 years of injection. The same volume of CO_2 is injected in both cases but the vertical mobility is different in both cases. The reservoir slice is taken in Y-direction.

7 Simulation Results of Faults Transmissibility

There are eight faults inferred at the top of the reservoir from the 3-D seismic interpretations and are assumed to be vertical within the reservoir. Two main faults cross the storage complex from the reservoir to the overburden, which limit the south-eastward extension of the reservoir. These are the F11 (Ubierna fault), located at the southern part, and the F9 (East fault) located at the eastern part of the Hontomín site. The location of all the eight faults and migration distance of CO_2 plume from the injection well in 200 years of gas injection for case base_21 is shown in Figure 27.

The transmissibilities of all the faults were varied from 0 (complete barrier) to 1 (fully transmissive) in a sensitivity study. The fault transmissibility multiplier values along with the simulation case name that were used in the sensitivity study are given in Table 5. After 200 years of simulated time, the CO_2 plume could still not reach the boundaries of the reservoir at the injection rate which was used in the historical data. The gas and water injection rates in the predictive simulation study plan followed the in-situ injection strategy as given in the historical data. The effect of transmissibility of all the faults on migration of CO_2 plume could not be observed over 200 years of gas injection. Only the influence of the F11 and R4+5 faults was observed, which were located within the range of CO_2 plume spread.

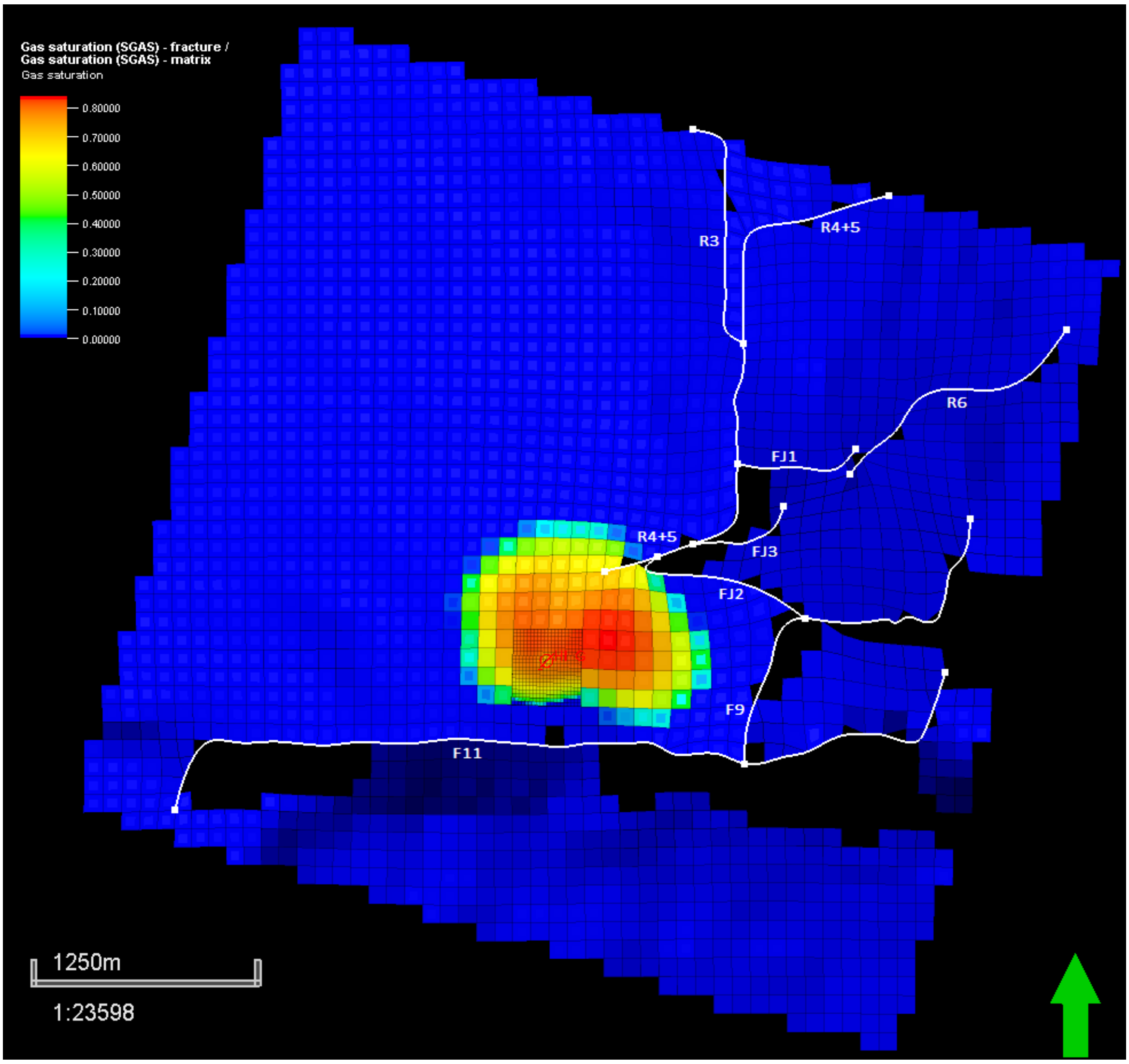

Figure 27. Location of faults in Sopeña Formation and migration distance of CO_2 plume from the injection well in 200 years of gas injection.

Table 5. Faults names as defined in the Geological model and transmissibility multiplier in respective simulated cases in sensitivity study.

Cases	TM_F11	TM_F9	TM_FJ1	TM_FJ2	TM_FJ3	TM_R3	TM_R6	TM_R4+5
BASE_20	0	0	0	0	0	0	0	0
BASE_21	1	0	0	0	0	0	0	0
BASE_22	0	1	0	0	0	0	0	0
BASE_23	0	0	1	0	0	0	0	0
BASE_24	0	0	0	0	0	0	0	0
BASE_25	0	0	0	1	0	0	0	0
BASE_26	0	0	0	0	1	0	0	0
BASE_27	0	0	0	0	0	1	0	0
BASE_28	0	0	0	0	0	0	1	0
BASE_29	0	0	0	0	0	0	0	1
BASE_30	1	1	1	1	1	1	1	1

The influence of the transmissibility of fault F11 (Ubierna fault) on the migration of the CO_2 plume was greater than for the fault R4+5 in the given scenario. It was observed that the build-up and reservoir pressures gradually decreased when the Ubierna fault was fully transmissive and this trend of pressure decline was continuously decreasing as long as gas was being injected and flowing through the fault. In contrast, the reservoir and injection pressures slightly decreased when fault R4+5 was made fully transmissive. The influence of both faults on the pressures can be seen in Figure 28 when both faults are fully transmissive compared to a completely sealed state. Build-up and reservoir pressures increased to 162 and 155 bars respectively in 200 years of gas injection at historic injection rate when all the faults were completely sealing faults.

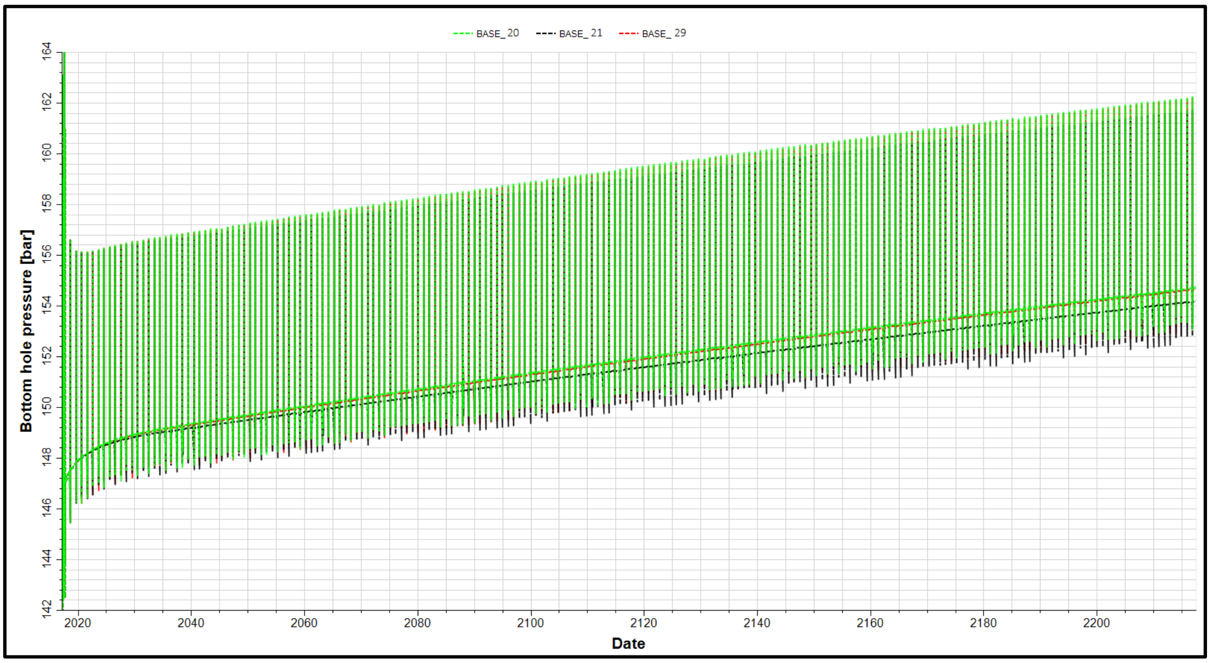

Figure 28. Influence of fault F11 and R4+5 transmissibility on reservoir and injection pressure compared to fully sealing case in 200 years of gas injection. The Cases base_21 and base_29 represent the fault F11 and R4+5 respectively when they are fully transmissive compared to base_20 which shows fully sealing state.

Conclusion

Geological heterogeneities influenced the direction of CO_2 plume migration as well as the reservoir storage capacity. In particular, a change in matrix porosity significantly changed the storage capacity compared to reservoir pressure. The influence of permeability heterogeneity on reservoir storage capacity and direction of CO_2 plume migration was observed and assessed by change in reservoir pressure. In this simulation study reservoir flow control mode was selected to match the simulated pressure with the observed pressure according to the industry norms and this was also continued for the prediction phase. Therefore, reservoir storage capacity was observed by difference in pressure response among the simulated cases instead of direct calculation from the injected volumes. It was found that the reservoir storage capacity significantly changed by changing the matrix permeability. For instance, at a similar reservoir pressure of 14800 kPa the case base_41 with high permeability distribution among the layers can store 2.9×10^5 tons of CO_2 which is 6.4 times more compared to the case base_31 which stored 4.5×10^4 tons and it has lowest permeability distribution among the layers.

It was observed that gas plume migrates in the direction of high matrix and fracture permeability as expected. However, the plume migration distance from the injection well is different at similar percent change in fracture and matrix permeability. This means that the plume migration distance from the injection well is different when the degree of permeability change in the Z-direction for matrix and fractures is similar. Plume spread was slightly larger when matrix permeability was changed instead of for fractures in Z-direction, when the absolute change in permeability was same for both cases. However, the plume spread away from the injection well was similar when the change in horizontal permeability of matrix and fractures was similar.

Thus, it was important to preserve the fracture permeability in simulation model according to the fracture density which observed in the real field during history matching process. These settings apply on prediction phase when large amount of CO_2 was injected for a longer period of time. A different distribution of petrophysical properties, especially permeability, in the model could mislead regarding the direction of plume migration in the long-term injection plan. The effect of the transmissibility of all the eight faults on migration of plume and reservoir pressure could not be observed over 200 years of gas and brine injection. However, the effect of the F11 (Ubierna fault) and R4+5 faults transmissibility on reservoir pressure were sensed and classified as marginal. In the sensitivity study the injection rate was set equal to the average in-situ injection rate to explore the impact of fault transmissibility on reservoir pressure and plume migration. However, at that injection rate, a variation in fault transmissibility multiplying factor from complete sealing to fully transmissive scenarios had no noticeable impact on reservoir pressure, except for Faults F11 and R4+5.

Glossary

B_w	Water formation volume factor (bbl/STB)
C_w	Water isothermal compressibility (bar^{-1})
CO_2	Carbon dioxide
μ_w	Water viscosity (cP)
K_h	Horizontal permeability
K_v	Vertical permeability
K_{fx}	Fracture permeability in x-direction
K_{fY}	Fracture permeability in y-direction
K_{fZ}	Fracture permeability in z-direction
Kf_{eff_X}	Fracture effective permeability in x-direction
Kf_{eff_Y}	Fracture effective permeability in y-direction
Kf_{eff_Z}	Fracture effective permeability in z-direction
$Km_{\_h}$	Matrix effective permeability in horizontal direction
$Km_{\_Z}$	Matrix effective permeability in vertical direction
kPa	Kilo Pascal
Kv/kh	Vertical to horizontal permeability ratio
ϕ_f	Fracture porosity
ϕ_m	Matrix porosity
Fracture_Permx	Fracture permeability in x-direction
Fracture_Permy	Fracture permeability in y-direction
Fracture_Permz	Fracture permeability in z-direction
LGR	Local grid refinement
Matrix_Permh	Matrix permeability in horizontal direction
Matrix_Permz	Matrix permeability in vertical direction
TM	Transmissibility

References

1. Dag Bakkejord. “Re: Reminder.” Message to Sean Rigby and Muhammad Adeel Nasser Sohal. 02 April 2019. E-mail.

2. Daniel Knight. “RE: WAG Process Simulation Problem - Schlumberger CCC: ISSUE=122846 PROJ=93.” Message to Matteo Icardi and Muhammad Adeel Nasser Sohal. 29 April 2019. E-mail.

3. Daniel Knight. “CO2-Brine WAG model validation problem. - Schlumberger CCC: ISSUE=123392 PROJ=93.” Message to Matteo Icardi and Muhammad Adeel Nasser Sohal. 20 May 2019. E-mail.

4. Hassanzadeh, Hassan, Mehran Pooladi-Darvish, Adel M. Elsharkawy, David W. Keith, and Yuri Leonenko. "Predicting PVT data for CO2–brine mixtures for black-oil simulation of CO2 geological storage." international journal of greenhouse gas control 2, no. 1 (2008): 65-77.

5. Shariatipour, Seyed mohammad, Gillian E. Pickup, Eric James Mackay, and Niklas Heinemann. "Flow Simulation of CO2 Storage in Saline Aquifers Using Black Oil Simulator." In Carbon Management Technology Conference. Carbon Management Technology Conference, 2012.

6. Hani. “[Ext] Ticket#1031902 - Schlumberger CCC ISSUE=1035068 PROJ=1” Message to Matteo Icardi and Muhammad Adeel Nasser Sohal. 03 July 2019. E-mail.

7. Amar Agnia. WAG E300 Validation Problem - Schlumberger CCC ISSUE=1036823 PROJ=1” Message to Matteo Icardi and Muhammad Adeel Nasser Sohal. 22 July 2019. E-mail.

8. Daniel Knight. Re: LGR Transmissibility Problem - Schlumberger CCC: ISSUE=125868 PROJ=93” Message to Matteo Icardi and Muhammad Adeel Nasser Sohal. 13 August 2019. E-mail.

9. Bennion, Brant, and Stefan Bachu. "Drainage and imbibition relative permeability relationships for supercritical CO2/brine and H2S/brine systems in intergranular sandstone, carbonate, shale, and anhydrite rocks." SPE Reservoir Evaluation & Engineering 11, no. 03 (2008): 487-496.

10. Dandekar, Abhijit Y. Petroleum reservoir rock and fluid properties. CRC press, 2013.

11. Skjaeveland, S. M., L. M. Siqveland, A. Kjosavik, W. L. Thomas, and G. A. Virnovsky. "Capillary Pressure Correlation for Mixed-Wet Reservoirs." SPE Reservoir Evaluation & Engineering 3, no. 01 (2000): 60-67.

12. Le Gallo, Yann, and de Dios, J. Carlos. "Geological Model of a Storage Complex for a CO_2 Storage Operation in a Naturally-Fractured Carbonate Formation." Geosciences 8.9 (2018): 354.

13. De Dios, J. Carlos, et al. "Hydraulic characterization of fractured carbonates for CO_2 geological storage: Experiences and lessons learned in Hontomín Technology Development Plant." International Journal of Greenhouse Gas Control 58 (2017): 185-200.

14. Journel, Andre G., and Charles J. Huijbregts. Mining geostatistics. Vol. 600. London: Academic press, 1978.

15. Ghanbari, So, Y. Al-Zaabi, G. E. Pickup, Eric Mackay, F. Gozalpour, and A. C. Todd. "Simulation of CO2 storage in saline aquifers." Chemical Engineering Research and Design84, no. 9 (2006): 764-775.

16. Ling, H. E., Zhao Lun, Li Jianxin, M. A. Ji, L. U. I. Ruilin, W. A. N. G. Shuqin, and Z. H. A. O. Wenqi. "Complex relationship between porosity and permeability of carbonate reservoirs and its controlling factors: A case study of platform facies in Pre-Caspian Basin." Petroleum Exploration and Development 41, no. 2 (2014): 225-234.

This deliverable is prepared as a part of ENOS project
More information about the project could be found at http://www.enos-project.eu

Be nice to the world!
Please consider to use and distribute this document electronically.

The project leading to this application has received funding from the European Union's Horizon 2020 research and innovation programme under grant agreement No 653718